Title: A potent synthetic nanobody targets RBD and protects mice from SARS-CoV-2 infection

Authors: Tingting Li[1,2,#], Hongmin Cai[1,2,#], Hebang Yao[1,2,#], Bingjie Zhou[2,3,#], Ning Zhang[4,#], Yuhuan Gong[2], Yapei Zhao[2,3], Quan Shen[4], Wenming Qin[5], Cedric A.J. Hutter[6], Yanling Lai[1,2], Shu-Ming Kuo[3], Juan Bao[1], Jiaming Lan[3], Markus A. Seeger[6], Gary Wong[3,7*], Yuhai Bi[2,4,*], Dimitri Lavillette[3,8*], Dianfan Li[1,*]

Affiliation: [1]State Key Laboratory of Molecular Biology, CAS Center for Excellence in Molecular Cell Science, National Center for Protein Science Shanghai, Shanghai Institute of Biochemistry and Cell Biology, Chinese Academy of Sciences (CAS), 320 Yueyang Road, Shanghai 200030, China.

[2]University of CAS, Beijing 101408, China

[3]CAS Key Laboratory of Molecular Virology & Immunology, Institut Pasteur of Shanghai CAS, 320 Yueyang Road, Shanghai 200031, China.

[4]CAS Key Laboratory of Pathogenic Microbiology and Immunology, Institute of Microbiology, Center for Influenza Research and Early-warning (CASCIRE), CAS-TWAS Center of Excellence for Emerging Infectious Diseases (CEEID), CAS, Beijing 100101, China

[5]National Facility for Protein Science in Shanghai, Shanghai Advanced Research Institute (Zhangjiang Laboratory), CAS, Shanghai, 201210, China.

[6]Institute of Medical Microbiology, University of Zurich, Zurich, Switzerland.

[7]Département de microbiologie-infectiologie et d'immunologie, Université Laval, Québec, QC, Canada

[8]Pasteurien College, Soochow University, Jiangsu, China.

[#]These authors contributed to the work equally.

[*]**Correspondence:** dianfan.li@sibcb.ac.cn; dlaville@ips.ac.cn; beeyh@im.ac.cn; garyckwong@ips.ac.cn

ABSTRACT

SARS-CoV-2, the causative agent of COVID-19[1], recognizes host cells by attaching its receptor-binding domain (RBD) to the host receptor ACE2[2-7]. Neutralizing antibodies that block RBD-ACE2 interaction have been a major focus for therapeutic development[8-18]. Llama-derived single-domain antibodies (nanobodies, ~15 kDa) offer advantages including ease of production and possibility for direct delivery to the lungs by nebulization[19], which are attractive features for bio-drugs against the global respiratory disease. Here, we generated 99 synthetic nanobodies (sybodies) by *in vitro* selection using three libraries. The best sybody, MR3 bound to RBD with high affinity (K_D = 1.0 nM) and showed high neutralization activity against SARS-CoV-2 pseudoviruses (IC_{50} = 0.40 μg mL^{-1}). Structural, biochemical, and biological characterization of sybodies suggest a common neutralizing mechanism, in which the RBD-ACE2 interaction is competitively inhibited by sybodies. Various forms of sybodies with improved potency were generated by structure-based design, biparatopic construction, and divalent engineering. Among these, a divalent MR3 conjugated with the albumin-binding domain for prolonged half-life displayed highest potency (IC_{50} = 12 ng mL^{-1}) and protected mice from live SARS-CoV-2 challenge. Our results pave the way to the development of therapeutic nanobodies against COVID-19 and present a strategy for rapid responses for future outbreaks.

INTRODUCTION

The coronavirus disease that emerged in early December 2019 (COVID-19)[1] poses a global health and economic crisis[20]. The causative agent, SARS-CoV-2, uses its Spike protein (S) to recognize receptors on host cells, an initial step for viral infection[2,3,21,22]. Key to this virus-host interaction is the binding between the S receptor-binding domain (RBD) and the host ACE2 protein[4-7]. Therefore, the RBD has been a primary target for neutralizing antibodies[8-13,23] to block ACE2-binding.

Llama-derived nanobodies are generally more heat stable, easier and less expensive for production, and more amenable to protein engineering compared to conventional antibodies[24]. As single-chain antibodies, nanobody libraries are less complex to construct and screen, enabling *in vitro* selection of high-affinity binders in relative short time, typically 2-4 weeks[25-30]. Recently, several nanobody therapeutics, including the caplacizumab approved by the US Food and Drug Administration, have been developed for a variety of immune diseases[31]. Of relevance to SARS-CoV-2, nanobodies can survive nebulization and an inhaler nanobody drug (ALX-0171) has gone into clinical trials for the treatment of the Respiratory Syncytial Virus[31]. Recent weeks have witnessed the generation of nanobodies that neutralize SARS-CoV-2 from several independent groups[14-18]. However, the *in vivo* efficacy of such nanobodies remains to be investigated.

Here, we report our efforts in selection and engineering synthetic nanobodies (sybodies)[26] that are highly potent against SARS-CoV-2, using biochemical and structural approaches. For the first time, we demonstrate that nanobodies can protect mice from live SARS-CoV-2 infection. Our results form a preliminary basis for the development of nanobody therapeutics for COVID-19.

RESULTS AND DISCUSSION

Generation of high-affinity neutralizing sybodies against SARS-CoV-2

SARS-CoV-2 S-RBD binders were selected by performing one round of ribosome display using three high-diversity libraries (Concave, Loop, and Convex)[26,27], and three rounds of phage display using the RBD as the bait under increasingly stringent conditions. Subsequent ELISA (**Extended Data Fig. 1**) identified 80, 77, and 90 positive clones, corresponding to 62, 19, and 18 unique binders from the Concave, Loop, and Convex library, respectively (**Extended Data Table 1**). Eighty sequencing 'first-comers'

of the 99 sybodies were further screened by a convenient fluorescence-detector size exclusion chromatography (FSEC) assay using crude extract from sybody-expressing clones. This identified 28 (36%) sybodies, including 9 Concave (21%), 9 Loop (50%), and 10 Convex (56%) binders that caused earlier retention of the fluorescein-labeled RBD (**Extended Data Fig. 2A, Extended Data Table 1**).

The same 80 sybodies were also screened for neutralization activity against retroviral pseudotypes harboring the SARS-CoV-2 S protein. Using 50% neutralization at 1 μM concentration as a cut-off, 11 Concave (26%), 13 Loop (68%), and 10 Convex (56%) sybodies were identified as positive (**Extended Data Fig. 3A**). The high positive rates suggest high efficiency of the *in vitro* selection platform. Of note, none of the sybodies showed noticeable neutralization activities for the closely related SARS-CoV pseudovirus (**Extended Data Fig. 3B**), indicating high specificity.

Six FSEC-positive neutralizing sybodies, namely SR4 (1), MR3 (31), MR4 (9), MR17 (1), LR1 (31), and LR5 (19) (S, M, L refers to Concave, Loop, and Convex sybodies respectively; brackets indicate ELISA redundancy), were characterized in more detail as follows. They could be purified from *Escherichia coli* with high yield (**Fig. 1A**), formed complexes with RBD on gel filtration (**Extended Data Fig. 2B**), displayed ultra-high thermostability (**Fig. 1A, Extended Data Fig. 2C**) as originally designed [26], and bound to the RBD with relatively high affinity (**Fig. 1A, Extended Data Fig. 4)**, with K_D ranging from 83.7 nM (MR17) to 1.0 nM (MR3). Consistent with its highest affinity, MR3 showed the slowest off-rate (2.3×10^{-4} s^{-1}). Using neutralization assays, we determined IC_{50} of the six sybodies (**Fig. 1B**). MR3 was the most potent (IC_{50} of 0.40 μg mL^{-1}), indicating a largely consistent trend between neutralization potency and binding kinetics (affinity and off-rate).

Structure of sybody-RBD complexes

To gain mechanistic insights into neutralization, we performed crystallization trials for several RBD-sybody complexes and obtained crystals for four. Crystals of SR4- and MR17-RBD diffracted to 2.15 Å and 2.77 Å resolution respectively and allowed structure determination (**Extended Data Table 2**). Crystals for MR3- and MR4-RBD did not diffract beyond 8.0 Å despite our optimization efforts.

A

Sybody	Yield (mg L^{-1})	$F_{99\,°C}$ / $F_{4\,°C}$	K_D (nM)	K_{on} (M^{-1} s^{-1})	K_{off} (s^{-1})	IC_{50} (μg mL^{-1})
SR4	16.3	0.58	14.5	9.9×10^4	1.4×10^{-3}	5.90
MR3	18.8	0.70	1.0	2.3×10^5	2.3×10^{-4}	0.40
MR4	29.7	0.73	23.3	2.7×10^5	6.4×10^{-3}	0.74
MR17	20.2	0.80	83.7	1.2×10^5	9.7×10^{-3}	12.32
LR1	16.9	N.D.	47.5	2.0×10^5	9.6×10^{-3}	2.34
LR5	27.3	N.D.	22.8	1.4×10^5	3.2×10^{-3}	2.06

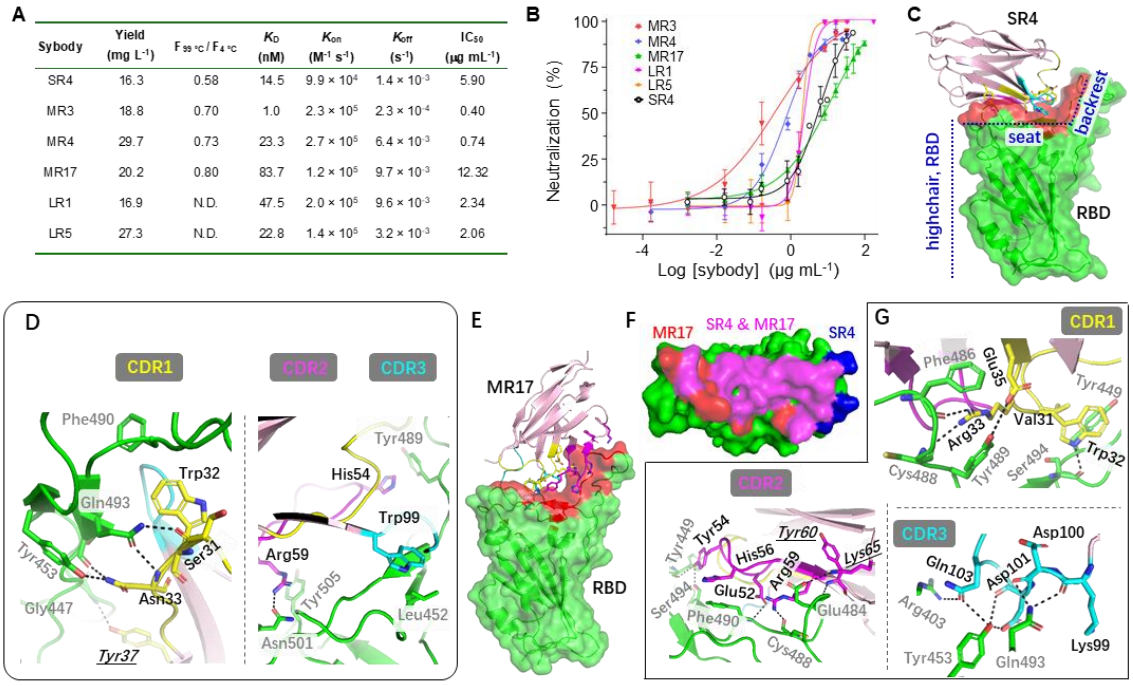

Fig. 1. Biochemical and structural characterization of neutralizing sybodies. (**A**) Summary of the characterization. Yield refers to purification from 1 L of culture. Fractional fluorescence (F) indicates remaining gel filtration peak intensity of sybodies after heating at 99 °C for 20 min. N. D., not determined. (**B**) Neutralization assay. SARS-CoV-2 pseudoviruses were pre-incubated with different concentration of sybodies before infection of VeroE6-hACE2 cells. The rate of infection was measured by fluorescence-activated cell sorting (FACS). IC_{50} was obtained by Sigmoidal fitting of the percentage of neutralization. Data are from three independent experiments. (**C**) The overall structure of SR4 (pink cartoon) in complex with RBD (green surface) which resembles a short backrest high chair. The binding surface is highlighted red. (**D**) SR4 CDR1 (yellow), CDR2 (magenta), and CDR3 (cyan) all contributed to the binding. Underlining italics label the framework residue Tyr37. (**E**) The overall structure of the MR17 (pink cartoon) in complex with RBD (green surface). (**F**) The overlap (magenta) between the SR4- (blue) and MR17- (red) interacting surfaces on RBD. (**G**) All three CDRs contributed to the binding with RBD (green). Underlining italics label the framework residues Lys65 and Tyr60. Dashed lines indicate H-bonding or salt-bridges between atoms that are <4.0 Å apart. Black texts label sybody residues and grey texts label RBD residues.

The RBD structure resembles a short backrest high chair and SR4 binds to both the 'seat' and 'backrest' (**Fig. 1C**) with a surface area[32] of 727.37 Å^2 with modest electrostatic complementarity (**Extended Data Fig. 5A**). Of note, SR4 binds sideways, as intended by design of the Concave sybody library[26]. All three CDRs contributed to

142 the binding through hydrophobic interactions and H-bonding that involves both side
143 chains and main chains (**Fig. 1D**). In addition, Tyr37, a framework residue, also
144 participated binding by forming an H-bond with the RBD Gly447 backbone.
145

146 MR17 also binds to the RBD at the 'seat' and 'backrest' regions but approaches
147 the RBD at an almost perfect opposite direction of SR4 (**Fig. 1C, 1E**), indicating
148 divergent binding mode for these sybodies. The binding of MR17 to the RBD occurred
149 on an 853.94 $Å^2$ surface area with noticeable electrostatic complementarity (**Extended**
150 **Data Fig. 5B**). Interestingly, this surface was largely shared with the SR4 binding surface
151 (**Fig. 1F**). The interactions between MR17 and the RBD were mainly mediated by H-
152 bonding. Apart from the three CDRs, two framework residues, Lys65 and Tyr60,
153 interacted with the same RBD residue Glu484, via a salt bridge with its side chain, and
154 an H-bond with its main chain (**Fig. 1G**).
155
156
157 **Molecular mechanism for neutralization**

158 Structure alignment of SR4-, MR17- and ACE2-RBD[4] showed that both sybodies
159 engage with RBD at the receptor-binding motif (RBM) (**Fig. 2A, 2B)**. Superposing SR4
160 and MR17 to the S trimer showed both sybodies could bind to the 'up' conformation[2]
161 of RBD with no steric clashes (**Fig. 2C, 2D**), and to the 'down' conformation with only
162 minor clashes (**Extended Data Fig. 6**) owing to their minute sizes. Consistent with the
163 structure observation, both SR4 and MR17 inhibited the binding of ACE2 to RBD, as
164 revealed by bio-layer interferometry (BLI) assays (**Fig. 2E, 2F**).
165

166 To probe the epitope for MR3 without a structure, competitive BLI binding assays
167 were carried out. The results showed that MR3 could block ACE2 (**Fig. 2G**), and SR4
168 and MR17 (**Fig. 2H, 2I**), suggesting it also binds to at least part of the RBM, although
169 the possibility of allosteric inhibition remains to be investigated. Taken together, SR4
170 and MR17, and probably MR3, neutralize SARS-CoV-2 by competitively blocking the
171 ACE2-RBD binding.

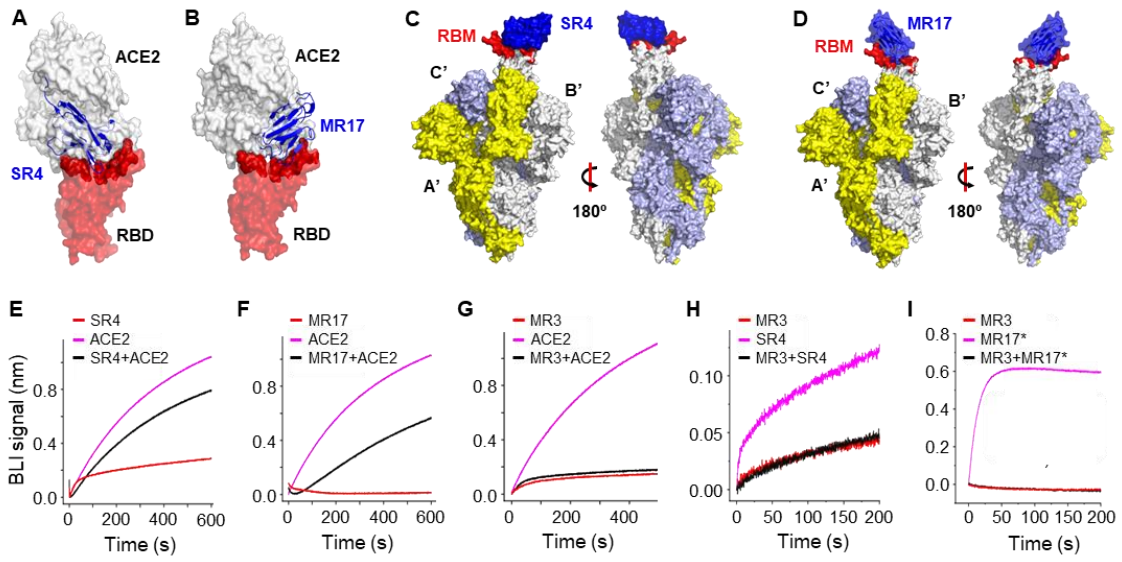

Fig. 2. Molecular basis for neutralization. (**A,B**) Alignment of the SR4- (**A**) or MR17- (**B**) RBD to the ACE2-RBD structure (PDB ID 6M0J)[4] reveals that SR4/MR17 (blue) binds RBD (red) at the motif (dark red) where ACE2 (white) also binds at. (**C,D**) Alignment of the SR4-RBD (**C**) and MR17-RBD (**D**) to the 'up' conformation of the RBD from the cryo-EM structure of the trimer S (PDB ID 6VYB)[2]. A'/B'/C' label three subunits. RBM (red) marks the ACE2-binding motif. (**E-G**) Competitive binding for the RBD between sybody and ACE2. A sensor coated with streptavidin was saturated with 2 μg mL^{-1} of biotinylated RBD. The sensor was then soaked in 200 nM of indicated sybody before further soaked in sybody-containing buffer with (black) or without (red) 25 nM of ACE2 for BLI signal recording. As a control, the ACE2-RBD interaction was monitored in the absence of sybodies (magenta). (**H-I**) Competitive BLI assay for the RBD between sybody pairs. A sensor with immobilized RBD was soaked in 200 nM of MR3 before further soaked in MR3-containing buffer with (black) or without SR4/MR17 (red). As a control, the SR4- and MR17-RBD interaction were monitored in the absence of MR3 (magenta). In (**I**), MR17* indicates a MR17 mutant (see below). Panels **E-I** share the same Y-axis title.

Sybody engineering increased affinity and neutralizing activity

Increasing valency is a common technique to enhance potency for nanobodies[18,31]. To this end, we engineered three types of divalent sybodies, including the biparatopic fusion of two different sybodies, the Fc-fusion and direct fusion of the same sybody.

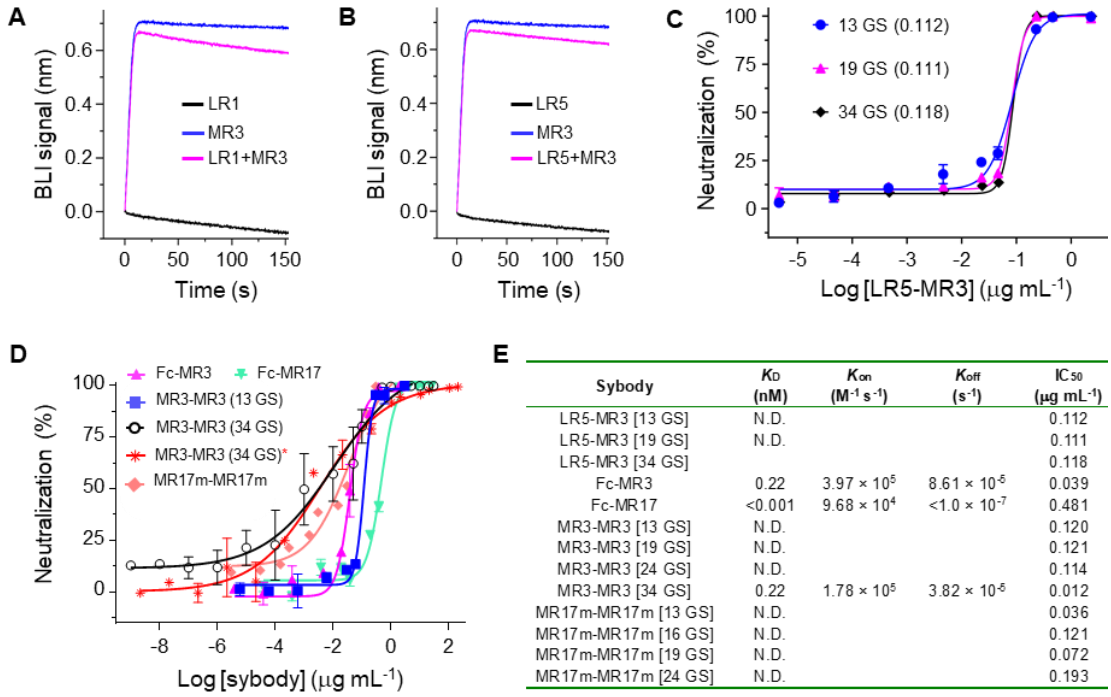

E

Sybody	K_D (nM)	K_{on} (M^{-1} s^{-1})	K_{off} (s^{-1})	IC_{50} (μg mL^{-1})
LR5-MR3 [13 GS]	N.D.			0.112
LR5-MR3 [19 GS]	N.D.			0.111
LR5-MR3 [34 GS]				0.118
Fc-MR3	0.22	3.97×10^5	8.61×10^{-5}	0.039
Fc-MR17	<0.001	9.68×10^4	$<1.0 \times 10^{-7}$	0.481
MR3-MR3 [13 GS]	N.D.			0.120
MR3-MR3 [19 GS]	N.D.			0.121
MR3-MR3 [24 GS]	N.D.			0.114
MR3-MR3 [34 GS]	0.22	1.78×10^5	3.82×10^{-5}	0.012
MR17m-MR17m [13 GS]	N.D.			0.036
MR17m-MR17m [16 GS]	N.D.			0.121
MR17m-MR17m [19 GS]	N.D.			0.072
MR17m-MR17m [24 GS]	N.D.			0.193

Fig. 3. Divalent engineering increased affinity and neutralizing activity. (**A,B**) Identification of two non-competing pairs, LR1/MR3 (**A**) and LR5/MR3 (**B**), for biparatopic constructs. For BLI assays, sensors coated with RBD were soaked in 200 nM of LR1 or LR5 before further soaked in LR1- or LR5-containing buffer with (magenta) or without (black) 100 nM of MR3. The MR3-RBD interaction profile was obtained in the absence of LR1 or LR5 (blue). (**C**) Neutralization assay of the biparatopic sybody LR5-MR3 with a GS linker of various length as indicated. Brackets indicate IC_{50} values in μg mL^{-1}. (**D**) Neutralization assays of divalent sybodies. The original SARS-CoV-2 was used for all assays except that the D614G mutant[33] was additionally tested for MR3-MR3 (red asterisk). (**E**) Summary of binding kinetics and neutralizing activities of the divalent sybodies. N.D., not determined.

For biparatopic fusion, we first identified two sybodies, namely LR1 and LR5 (**Fig. 3A, 3B**), that could bind RBD in addition to MR3 using the BLI assay. As LR5 showed higher affinity and neutralization activity than LR1 (**Fig. 1A**), we fused this non-competing sybody to the N-terminal of MR3 with various length of GS linkers ranging from 13 to 34 amino acids (**Extended Data Table S1**). Interestingly, the linker length had little effect on neutralization activity and these biparatopic LR5-MR3 sybodies were more potent than either sybodies alone (**Fig. 1A**) with an IC_{50} of 0.11 μg mL^{-1} (**Fig. 3C**). LR5-MR3 may be more tolerant to escape mutants[34-37] owing to its ability to recognize two distinct epitopes.

For Fc-fusion, both MR3 and MR17 were attached to the dimeric human IgG Fc. This decreased IC_{50} by 10 folds for Fc-MR3 (39 ng mL^{-1}) and 25 folds Fc-MR17 (0.48 μg

220 mL^{-1}), respectively (**Fig. 3D, 3E**). Consistently, the Fc fusion increased the apparent
221 binding affinity for both sybodies, with a K_D of 0.22 nM for Fc-MR3 and less than 1 pM
222 for Fc-MR17 (**Extended Data Fig. 4H, 4I**). Note, however, Fc-MR17 did not gain as much
223 neutralization potency as for the apparent binding affinity.
224
225 For direct fusion, MR3 and a rationally designed MR17 mutant (MR17m,
226 **Extended Data Fig. 7**) that showed comparable IC_{50} with MR3 by a single mutation
227 K99Y (0.50 μg mL^{-1}, **Extended Data Fig. 7G**) were individually linked together via GS
228 linkers with variable length ranging from 13 to 34 amino acids (**Extended Data Table**
229 **1**). The optimal construct for MR17m-MR17m had the shortest linker (13-GS) (**Fig. 3D,**
230 **3E**). By contrast, optimal neutralization activity was observed with the longest linker
231 (34-GS) for MR3-MR3 (**Fig. 3D, 3E**). Again, MR3-MR3 was superior compared to
232 MR17m-MR17m, showing a 2-fold higher neutralization activity with an IC_{50} of 12 ng
233 mL^{-1} (**Fig. 3E**). Compared to the monovalent MR3 (IC_{50} of 0.40 μg mL^{-1}), the divalent
234 engineering increased the potency by over 30 folds. Notably, MR3-MR3 showed similar
235 activity to inhibit pseudotypes harboring the original SARS-CoV-2 S or the current
236 dominant and more infectious mutant D614G S (ref. [33]) (**Fig. 3D**).
237
238 **Divalent MR3 protects mice from COVID-19**
239
240 The most potent divalent sybody (MR3-MR3) was chosen to investigate the
241 potential of nanobodies to protect mice from SARS-CoV-2 infection. Nanobodies have
242 very short serum half-lives of several minutes due to their minute size[38]. To circumvent
243 this, we fused MR3-MR3 to the N-terminus of an albumin-binding domain (ABD)[39]
244 which has been known to extend the circulating half-life of its fusion partners by
245 increase in size and preventing intracellular degradation[31]. Conveniently, we expressed
246 MR3-MR3-ABD in *Pichia pastoris*, which is the preferred host to express nanobody
247 therapeutics owing to its robustness and its endotoxin-free production. Small-scale
248 expression of MR3-MR3-ABD showed a secretion level of ~250 mg L^{-1} with an apparent
249 purity of >80% without purification (**Fig. 4A**). Note, this experiment was carried out
250 using a shaker which gave cell density of OD_{600} of 16. Given its ability to grow to OD_{600}
251 of 500 without compromising yield, the expression level of MR3-MR3-ABD may reach
252 7.5 g L^{-1} in fermenters. The potential for simple and high-yield production is especially
253 attractive for the pandemic at a global scale.
254
255 Importantly, MR3-MR3-ABD could bind to the human albumin (**Fig. 4B**) while
256 retaining its ability to bind RBD (**Fig. 4C**) and to neutralize SARS-CoV-2 pseudotypes
257 harboring either past (614D) and current (614G)[33] SARS-CoV-2 S (**Fig. 4D**). As designed,

258 a serum virus neutralization assay showed that the addition of the albumin binding
259 domain to the divalent MR3 (MR3-MR3-ABD) extended its *in vivo* stability, displaying
260 neutralization activity up to 24 h post injection contrary to the other forms (**Extended**
261 **Data Fig. 8A**). The body weight measures, and the microscopic histopathology analysis
262 did not reveal any toxicity for the nanobodies for 6 days (**Extended Data Fig. 8B, 8C**).
263

264 To test the *in vivo* antiviral efficacy of MR3-MR3-ABD, C57BL/6J female mice, aged
265 6-8 weeks old, were first sensitized to SARS-CoV-2 infection using an adenovirus
266 expressing the human ACE2 receptor[40] at 5 days before challenge. Mice were infected
267 via the intranasal route with 5 x 10^6 median tissue culture infectious dose ($TCID_{50}$) of
268 SARS-CoV-2, and then administered a single dose of 25 mg kg^{-1} MR3-MR3-ABD via the
269 intraperitoneal route at 12 h after virus challenge. A control C57BL/6J group were
270 given PBS as a mock treatment. Compared to the control group, the lung viral titers of
271 the sybody group was 50-fold lower than the PBS group, when assessed at 3 dpi (**Fig.**
272 **4E**). This efficacy is similar to the existing human monoclonal antibody CB6 (2
273 injections, 50-fold, in rhesus macaques)[41] and better than that for 1B07 (1 injection,
274 10-fold, mice)[42] when compared under similar sampling points.
275

276 Histopathological examination revealed that the infected mice in the PBS-treated
277 group displayed moderate bronchopneumonia lesions, with a large number of
278 inflammatory cell infiltrations around the bronchioles and terminal bronchioles. The
279 alveolar walls were thickened, a large number of inflammatory cells were exuded in
280 the interstitium, accompanied by red blood cell exudation. In addition, part of the
281 alveolar cavity showed compensatory expansion (**Fig. 4F**). In contrast, the lungs of
282 sybody-treated mice showed normal alveolar wall structures, and only displayed mild
283 bronchopneumonia, with a small amount of inflammatory cell infiltration around the
284 bronchioles (**Fig. 4F**). Taken together, the significant reduction of the lung viral load
285 and the severity of lung damage demonstrated the *in vivo* efficacy of the MR3-MR3-
286 ABD against authentic SARS-CoV-2 infection.
287

288 In summary, the *in vitro* platform was efficient in generating neutralizing sybodies
289 (the selection process took 2 weeks). Structural and biochemical studies suggested an
290 antagonistic mechanism to block the ACE2-RBD interaction. Protein engineering
291 yielded various forms of sybody with higher affinity, neutralization activity, and *in vivo*
292 stability. Using the most potent construct, we have in the first time demonstrated that
293 nanobodies can provide post-exposure protection of mice from SARS-CoV-2 infection.
294 Our results should encourage development of nanobody therapeutics to fight COVID-
295 19 or future viral outbreaks.

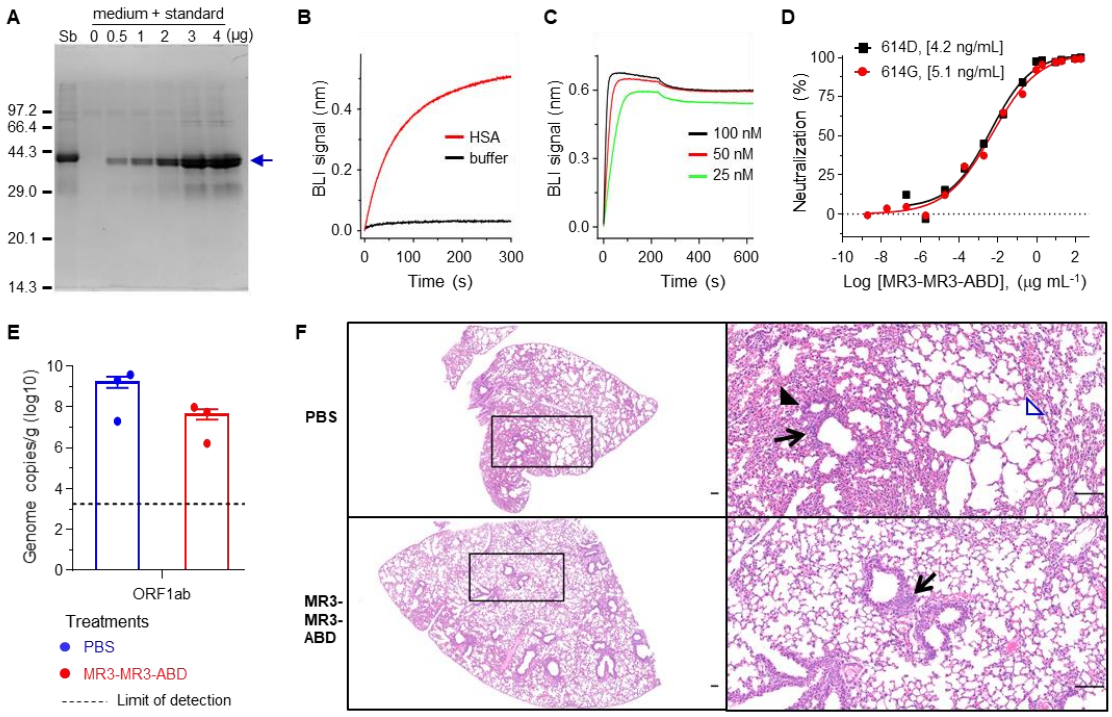

296

297 **Fig. 4. The Divalent MR3 sybody protects mice from live SARS-CoV-2 challenge.** (**A**)
298 Coomassie Blue staining of SDS-PAGE for MR3-MR3-ABD (arrow) expression in pichia.
299 Based on the standards, the yield (Lane Sb) was semi-quantified as 0.25 g L^{-1}. (**B,C**) BLI
300 binding assays show that MR3-MR3-ABD bind to human serum albumin (HSA) (**B**) and
301 RBD (**C**). RBD-coated sensors were incubated with 200 nM of HSA (**B**) or indicated
302 concentrations of MR3-MR3-ABD (**C**) for single monitoring. (**D**) Neutralization assay of
303 MR3-MR3-ABD. Data are from one representative experiment of two independent
304 experiments. (**E**) Lung viral loads as determined by PCR from infected mice at 3 dpi. (**F**)
305 Histopathology of lungs from infected mice at 3 dpi. The arrows denote inflammatory
306 cell infiltration. A black triangle indicates typical red blood cell exudation, and a blue
307 triangle indicates typical compensatory expansion of the alveolar cavity. The left
308 panels denote an overview of the lung at 10x magnification. The right panels denote
309 the expanded view of the black boxes in the left panels, at 100x magnification. Bars =
310 100 μm.

ACKNOWLEDGMENTS

We thank the staff members of the Large-scale Protein Preparation System for equipment maintenance and management, and staff scientists at the SSRF-BL19U1 beamline at National Facility for Protein Science (Shanghai) for technical support and assistance. We thank Dr. Zhipu Luo at Soochow University (China) for helpful discussions regarding data processing. This work has been supported by the Strategic Priority Research Program of CAS (XDB37020204, D.Li; XDB29010102 & XDA19090118, Y.B.), Key Program of CAS Frontier Science (QYZDB-SSW-SMC037, D.Li), CAS Facility-based Open Research Program, the National Natural Science Foundation of China (31870726, D.Li; 31870153, D.La.; 32041010, Y.B.), the One Belt and One Road major project for infectious diseases (2018ZX10101004-003, J.L., G.W.), National Key R&D Program of China (2020YFC0845900, D.La.), CAS president's international fellowship initiative (2020VBA0023, D.La.), Natural Science Foundation of Shanghai (20ZR1463900, G.W.), and Shanghai Municipal Science and Technology Major Project (20431900402, D.La.). Y.B. is supported by the NSFC Outstanding Young Scholars (31822055) and Youth Innovation Promotion Association of CAS (2017122). G.W. is supported by a G4 grant from IP, FMX and CAS.

AUTHOR CONTRIBUTIONS

T.L., H.C., and H.Y. selected sybodies under the supervision of C.A.J.H. and M.A.S.. T.L., H.C., and H.Y. purified and crystalized protein complexes with assistance from Y.L.. H.Y. biochemically characterized sybodies. B.Z. and Y.Z. performed neutralization assays under the supervision of D.La. N.Z., Y.G. and Q.S. performed animal experiments under supervision of Y.B. and G.W.. W.Q. collected X-ray diffraction data. B.J. helped with molecular cloning. S.K. performed half-life assays in mice. J.L. and G.W. developed reagents for the neutralizing assays. G.W. developed the mice model used for in vivo studies. D.Li. conceived the project, solved the structures, analyzed data, and wrote the manuscript with inputs from H.Y., T.L., H.C., B.Z., G.W., Y.B., M.A.S., and D.La.

CONFLICT OF INTEREST

The authors declare no conflict of interest.

SUPPLEMENTARY MATERIALS

Materials and Methods

Extended Data Table 1-2

Extended Data Fig. 1-8

MATERIALS AND METHODS

Protein expression and purification – *SARS-CoV-2 S-RBD for sybody selection*

The construct for the RBD with an Avi-tag for biotinylation was made by fusing DNA, from 5'- to 3'-end, of the encoding sequence for the honey bee melittin signal peptide (KFLVNVALVFMVVYISYIYAA), a Gly-Ser linker, residues of 330-541 of the SARS-CoV-2 spike protein (Uniprot P0DTC2), a Gly-Thr linker, the 3C protease site (LEVLFQGP), a Gly-Ser linker, the Avi tag (GLNDIFEAQKIEWHE), a Ser-Gly linker, and a deca-His tag, into a pFastBac-backbone vector by Gibson assembly[43]. Baculoviruses were generated using standard Bac-to-Bac protocols and expression was achieved by infecting *Trichoplusia ni* High Five suspension cells at 2×10^6 cells per milliliter for 48-60 h at 27 °C in flasks. The medium from 1 L of culture was filtered through a 0.22-μm membrane and incubated with 3.0 mL of Ni-Sepharose Excel (Cat 17-3712-03, GE Healthcare) in the presence of 20 mM of imidazole for 2-3 h at 4 °C with mild agitation. The beads were washed with 10 column volume (CV) of 20 mM imidazole in **Buffer A** (150 mM NaCl, 20 mM Tris HCl pH 8.0). The RBD was eluted using 300 mM of imidazole in **Buffer A**. For biotinylation[26,27], the purified RBD with the Avi-tag intact (0.8 mg mL^{-1}) was incubated with 5 mM ATP, 10 mM magnesium acetate, 43.5 μM biotin, 22 μg mL^{-1} home-purified BirA in 3.2 mL volume and incubated at 4 °C for 16 h. Biotinylated RBD was concentrated using a 10-kDa cut-off membrane concentrator to ~3 mg mL^{-1} before loaded onto a Superdex Increase 200 10/300 GL column for size exclusion chromatography. Fractions containing the RBD were pooled, aliquoted, flash-frozen in liquid nitrogen, and stored at -80 °C before use.

Protein expression and purification – *SARS-CoV-2 S-RBD for crystallization*

For protein crystallization, the RBD was purified as above. Both the Avi-tag and the His-tag were removed by 3C protease digestion as follows. The pooled elution from Ni-Sepharose Excel column was desalted to remove imidazole using a desalting column (Cat. 732-2010, Bio-Rad) pre-equilibrated in **Buffer A**. The desalted RBD was mixed with home-purified His-tagged 3C protease at 1:100 molar ratio (3C protease : RBD) at 4 °C for 16 h. The mixture was then passed through a Ni-NTA column which binds 3C protease, undigested RBD, and the cleaved His-tag. The flow-through fractions were collected and concentrated to 8-10 mg mL^{-1}. The protein was either used directly for crystallization, or flash-frozen in liquid nitrogen and stored at -80 °C before use.

For crystallization, fresh RBD or thawed from -80 °C was mixed with desired sybodies at 1:1.5 molar ratio (RBD:sybody). After incubation on ice for 30 min, the mixture was clarified by centrifugation before size exclusion chromatography.

389 Fractions containing the complex were pooled, concentrated to ~10-15 mg mL^{-1} before
390 crystallization trials.
391

392 **Protein expression and purification – *sybodies in Escherichia coli***

393 Sybodies were expressed with a C-terminally His-tag in *Escherichia coli* MC1061
394 cells. Briefly, cells carrying sybody genes in the vector pSb-init[26,27] were grown in
395 Terrific Broth (TB, 0.17 M KH_2PO_4 and 0.72 M K_2HPO_4, 1.2 %(w/v) tryptone, 2.4 %(w/v)
396 yeast extract, 0.5% (v/v) glycerol) supplemented with 25 mg L^{-1} chloramphenicol to
397 OD_{600} of 0.5 at 37 °C in a shaker-incubator at 220 rpm. The growth temperature was
398 lowered to 22 °C and the cells were allowed to grow for another 1.5 h before induced
399 with 0.02% (w/v) arabinose for 17 h. Cells were lysed by osmotic shock. Briefly, cells
400 from 1 L of culture were re-suspended in 20 mL of TES-high Buffer (0.5 M sucrose, 0.5
401 mM EDTA, and 0.2 M Tris-HCl pH 8.0) and incubated at 4 °C for 30 min. After this
402 dehydration step, cells were abruptly rehydrated with 40 mL of ice-cold MilliQ H_2O at
403 4 °C for 1 h. The periplasmic extract released by the osmotic shock was collected by
404 centrifugation at 20,000×g at 4 °C for 30 min. The supernatant was adjusted to contain
405 150 mM of NaCl, 2 mM of $MgCl_2$, and 20 mM of imidazole before added with Ni-NTA
406 resin that had been pre-equilibrated with 20 mM of imidazole in **Buffer A** (150 mM
407 NaCl and 20 mM Tris HCl pH 8.0). After batch-binding for 2 h, the beads were washed
408 with 30 mM imidazole, before eluted with 300 mM imidazole in **Buffer A**. The eluted
409 protein was either used directly or flash-frozen in liquid nitrogen and stored at -80 °C.
410

411 **Protein expression - sybody MR3-MR3-ABD in *Pichia pastoris***

412 The encoding gene for MR3-MR3-ABD (**Table S1**) was cloned into vector pPICZαC
413 (Invitrogen) immediately in frame with the α-factor signal peptide. To express MR3-
414 MR3-ABD in yeast, *Pichia pastoris* GS115 and SMD1168H were transformed with *Sac*I-
415 linearized plasmid and selected with 0.1 and 0.5 mg mL^{-1} zeocin on an YPDS agar plate
416 (1 %(w/v) yeast extract, 2 %(w/v) peptone, 2 %(w/v) glucose, 0.8 M sorbitol, 2 %(w/v)
417 agarose). Colonies (12 for each strain) were inoculated into 3 mL YPD liquid medium.
418 Cells were grown in a 30-°C incubator. After 24 h, cells were harvested, washed twice
419 with methanol-complex medium (BMMY), and suspended in BMMY medium at a final
420 OD_{600} of 4-5 for induction. Methanol was supplemented to the medium to 0.5 %(v/v)
421 every 24 h. After 3 days of expression, the medium was collected by centrifugation and
422 the secreted protein was used for SDS-PAGE analysis.
423

424 To quantify the expression level, the supernatant (10 μL) was loaded together
425 with known amount of MR3-MR3-ABD (purified from *E. coli*, 0.5, 1, 2, 3, and 4 μg) that

426 had been pre-mixed with medium from culture of untransformed GS115. The band
427 intensity was semi-quantified by densitometry analysis using theImage Lab 5.2
428 software (Bio-Rad).
429

430 **Protein expression and purification** – ***divalent sybodies in mammalian cells***

431 The encoding sequence of MR3 was cloned into a vector harboring the hinge and
432 Fc regions of IgG2 (**Table S1**, uniprot P01859) for secretion in mammalian cells. Expi293
433 cells at density of 2.3 million per milliliter were transfected with the plasmid (final
434 concentration of 2 mg L^{-1}) using linear polyethylenimine (average MW of 25 kDa, 4 mg
435 L^{-1}). Valproic acid was included at a final concentration of 2 mM. Cells were cultured in
436 a flask for 65 h. The supernatant was collected by centrifugation and filtered through
437 a 0.22-μm membrane. The filtrate from 2 L of culture was incubated with 3.2 mL
438 rProtein A beads (Cat SA012005, SmartLifesciences, China) for batch binding at 4 °C for
439 3 h. The beads were packed into a gravity column, washed with 20 CV of PBS buffer,
440 before eluted with 0.1 M glycine pH 3.0. The elution was quickly neutralized using 1 M
441 Tris HCl pH 8.0. The buffer was then exchanged to PBS using a desalt column.
442

443 **Sybody selection** – ***ribosome display and phage display***

444 Sybody selection was performed using a combination of ribosome display and
445 phage display[26,27]. *In vitro* translation of the 'Concave', 'Loop', and 'Convex' library was
446 performed according to the manufacturer's instruction (PURE*frex* 2.1 kit, Cat. PF213-
447 0.25-EX, Genefrontier, Chiba, Japan). A reaction mix containing 1.8 μL of nuclease-free
448 water, 4 μL of solution I, 0.5 μL of solution II, 1 μL of solution III, 0.5 μL of 10 mM
449 cysteine, 0.5 μL of 80 mM reduced glutathione, 0.5 μL of 60 mM oxidized glutathione,
450 and 0.5 μL of 1.875 mg mL^{-1} disulfide bond isomerase DsbC (DS supplement, Cat.
451 PF005-0.5-EX, Genefrontier) was warmed at 37 °C. After 5 min, 0.7 μL of mRNA library,
452 corresponding to 1.6×10^{12} mRNA molecules, was added to the pre-warmed mix for *in*
453 *vitro* translation at 37 °C for 30 min. The reaction was diluted with 100 μL ice-cold
454 **Panning Solution** (150 mM NaCl, 50 mM magnesium acetate, 0.05 %(w/v) BSA,
455 0.1 %(w/v) Tween 20, 0.5 %(w/v) heparin, 1 μL RNaseIn, and 50 mM Tris-acetate pH
456 7.4) and cleared by centrifugation at 20,000×g for 5 min at 4 °C. Biotinylated RBD was
457 added to the supernatant and the mixture was incubated on ice for 20 min.
458 Streptavidin beads (Dynabeads Myone Streptavidin T1) were added to pull-down the
459 complex consisting of nascent sybody binders, the stalled ribosome with the mRNA
460 encoding the binders, and biotinylated RBD. Selected mRNAs were purified and
461 reverse-transcripted into single-chain DNA with the primer 5'-
462 CTTCAGTTGCCGCTTTCTTTCTTG-3' using a reverse transcriptase (Cat 200436, Agilent).

463 The resulting cDNA library was purified using a DNA purification kit (Cat A740609.25,
464 Macherey-Nagal), and PCR-amplified using the primer pair 5'-
465 ATATGCTCTTCTAGTCAGGTTCAGCTGGTTGAGAGCG-3' and 5'-
466 TATAGCTCTTCATGCGCTCACAGTCACTTGGGTACC-3' for 'Concave' and 'Loop' library,
467 and the primer pair 5'-ATATGCTCT TCTAGTCAAGTCCAGCTGGTGGAATCG-3' and 5'-
468 TATAGCTCTTCATGCAGAAACGGTAACTTGGGT GCCC-3' for the 'Convex' library. The
469 product was gel-purified, digested with the Type IIS restriction enzyme *BspQ*I, and
470 ligated into the vector pDX_init[26,27] treated with the same enzyme. The ligation
471 product was then transformed into *E. coli* SS320 competent cells by electroporation to
472 generate libraries for phage display.
473
474 Three rounds of phage display were carried out. The first round was performed
475 in a 96-well plate coated with 60 nM neutravidin (Cat. 31000, Thermo Fisher Scientific).
476 Phage particles were incubated with 50 nM biotinylated RBD, washed, and released
477 from the plate by tryptic digestion with 0.25 mg mL^{-1} trypsin in the buffer containing
478 150 mM NaCl and 20 mM Tris-HCl pH 7.4. The selected phage particles were amplified,
479 and the second round of selection was performed by switching the immobilizing
480 matrix to 12 µL of MyOne Streptavidin C1 beads that were pre-incubated with 50 nM
481 biotinylated RBD. Before releasing the phage particles, the binders were challenged
482 with 5 µM non-biotinylated RBD to compete off the binders with fast off-rates. The
483 second selection was repeated with 5 nM of the RBD. After three rounds of selection,
484 the phagemid was sub-cloned into pSb_init vector by fragment-exchange (FX) cloning
485 and transformed into *E. coli* MC1061 for further screening at a single-colony level[26,27].
486

487 **Enzyme-linked immunosorbent assay (ELISA) – *sybody selection***

488 Single colonies carrying sybody-encoding genes in the vector pSb-init were
489 inoculated into 96-well plates. Cells were grown at 37 °C for 5 h in a shaking incubator
490 at 300 rpm before 1:20 diluted into 1 mL of fresh TB medium supplemented with 25
491 µg mL^{-1} chloramphenicol. Cells were induced with arabinose as mentioned earlier at
492 22 °C for 17 h before harvested by centrifugation at 3,220 g for 30 min. Cells were
493 resuspended in TES Buffer (20 % (w/v) sucrose, 0.5 mM EDTA, 0.5 µg/mL lysozyme, 50
494 mM Tis-HCl pH 8.0) and shaken for 30 min at room temperature (RT, 22-25 °C). To the
495 lysate, 1 mL of **TBS** (150 mM NaCl, 20 mM Tris-HCl pH 7.4) with 1 mM $MgCl_2$ was added.
496 The mixtures, still in the plate, were then centrifuged at 3,220 g for 30 min at 4 °C. The
497 supernatant containing sybodies was used directed for ELISA or FSEC assay (below).
498
499 For ELISA, Protein A was incubated with Maxi-Sorp plate 96 well (Cat. 442404,

500 Thermo Fisher) at 4 °C for 16 h. The solution was then removed and the plate was
501 blocked by 0.5 %(w/v) bovine serum albumin (BSA) in **TBS** buffer for 30 min at RT. The
502 plate was washed three times using **TBS** before added with anti-myc antibodies at
503 1:2,000 dilution in TBS-BSA-T buffer (TBS supplemented with 0.5 %(w/v) BSA and
504 0.05 %(v/v) Tween 20). The antibody was allowed to bind to protein A for 20 min at RT.
505 The plate was then washed three times with **TBST** (TBS supplemented with 0.05%
506 Tween 20). Myc-tagged sybody prepared above was added and incubated for 20 min
507 at RT. After washing three times with **TBST**, biotinylated RBD or MBP (the maltose-
508 binding protein, as a control) was added to each well to a final concentration of 50 nM.
509 After incubation for 20 min at RT, the solution was discarded and the plate was rinsed
510 three times with **TBST**. Streptavidin conjugated with horseradish peroxidase (HRP) was
511 added to each well (1:5,000, Cat S2438, Sigma). After incubation at RT for 30 min, the
512 plate was washed three times again with **TBST**. ELISA signal (absorbance at 650 nm)
513 was developed by adding 100 μL of developing buffer (51 mM Na_2HPO_4, 24 mM citric
514 acid, 0.006 %(v/v) H_2O_2, 0.1 mg mL^{-1} 3,3',5,5'-tetramethylbenzidine) followed by
515 incubation at RT.
516

517 **Sybody selection** ***– fluorescence-detection size-exclusion chromatography (FSEC)***

518 To rapidly characterize RBD binders without purification, we have developed an
519 analytic, fluorescence-detection size exclusion chromatography (FSEC)-based assay as
520 follows. Biotinylated RBD_{avi} was bound to streptavidin (Cat 16955, AAT Bioquest) which
521 was fluorescently labeled by fluorescein via amine coupling. The complex is named as
522 FL-RBD_{avi}. To 0.5 μM of FL-RBD_{avi}, cell lysate containing unpurified sybodies were
523 added to an estimated concentration of 0.019 mg mL^{-1}, assuming expression level of
524 20 mg L^{-1}. The mixture was loaded onto an analytic gel filtration column (Cat 9F16206,
525 Sepax) connected to an HPLC system equipped with a fluorescence detector (RF-20A,
526 Shimadzu). The profile was monitored by fluorescence at the excitation/emission pair
527 of 482/508 nm. Periplasmic extract without sybodies was used as negative control.
528 Binders can be identified based on earlier retention volume, presumably reflecting the
529 bigger size of the FL-RBD_{avi}-sybody complex than the FL-RBD_{avi} alone.

530

531 **Bio-layer interferometry assay**

532 The binding kinetics were measured using a bio-layer interferometry (BLI) assay
533 with an Octet RED96 system (ForteBio). Biotinylated RBD was immobilized on a SA
534 sensor (Cat 18-5019) that was coated with streptavidin by incubating the sensor in 2
535 μg mL^{-1} of RBD in **Kinetic Buffer** (0.005 %(v/v) Tween 20, 150 mM NaCl, 20 mM Tris

536 HCl pH 8.0) at 30 °C. The sensor was equilibrated (baseline) for 120 s, before incubating
537 with sybodies at various concentrations (association) for 120 s (for MR3) or 300 s (for
538 all the others). The concentrations for SR4 are 0, 250, 500, 1000, and 2000 nM. The
539 concentrations for MR17 are 0, 125, 250, 500, and 1000 nM. The concentrations for
540 MR3/MR4 are 0, 12.5, 25, 50, and 100 nM. The sensor was then moved into sybody-
541 free buffer for dissociation and the signal was monitored for 600 s. Data were fitted
542 for a 1:1 stoichiometry for K_D, K_{on}, and K_{off} calculations using the built-in software Data
543 Analysis 10.0.

544

545 For competition binding of the RBD between sybody and ACE2 (Cat 10108-H08B,
546 Sino Biological), the RBD was immobilized and the sensor was equilibrated as
547 abovementioned. The sensor was then saturated using 1 μM sybody and the system
548 was equilibrated for 180 s. After saturation, the sensor was moved into sybody
549 solutions (50 nM) with or without 25 nM ACE2. The association of ACE2 was monitored
550 for 600 s. As a control, the ACE2-RBD interaction was monitored using sensors without
551 sybody incubation.

552

553 For the binding assay of MR3-MR3-ABD with HSA, the sensor was coated with RBD
554 as described earlier before saturated by incubation in 200 nM MR3-MR3-ABD before
555 soaked with 200 nM HSA for BLI signal monitoring. A control experiment was carried
556 out in parallel but the sensor was incubated in buffer without MR3-MR3-ABD.

557

558 **Thermostability assay**

559 Thermostability assay of sybodies was carried out using fluorescence-detection
560 size exclusion chromatography[44]. Sybodies at 9 μg mL^{-1} in **Buffer A** (150 mM NaCl, 20
561 mM Tris HCl pH 8.0) were heated at 90 and 99 °C for 20 min. The heated samples and
562 the non-heated samples (4 °C) were analyzed the same way as described in the FSEC
563 assay above except that the intrinsic tryptophan fluorescence (Ex. 280 nm, Em. 350
564 nm) was monitored.

565

566 **Pseudotyped particle production and neutralizing assays**

567 The retroviral pseudotyped particles were generated by co-transfection of
568 HEK293T cells using polyethylenimine with the expression vectors encoding the
569 various viral envelope glycoproteins, the Murine leukemia virus core/packaging

570 components (MLV Gag-Pol), and a retroviral transfer vector harboring the gene
571 encoding the green fluorescent protein (GFP). The S Protein expressed by phCMV-
572 SARS-CoV and phCMV-SARS-CoV-2 has been truncated in the cytoplasmic tail by
573 adding a stop codon which removed 19 amino acids at the C-terminal. Supernatants
574 that contained pseudotyped particles were harvested 48 h post-transfection and
575 filtered through a 0.45-μm membrane before been used for neutralizing assays.
576
577 VeroE6-hACE2 cells (10^4 cells/well) were seeded in a 48-well plate and infected
578 24 h later with 100 μL of virus supernatant in a final volume of 150 μL. Sybodies were
579 pre-incubated with the pseudotype samples for 1 h at 37 °C prior to cell/virus co-
580 incubation. After 6 h of co-incubation, the supernatants were removed and the cells
581 were incubated in medium for 72 h at 37 °C. GFP expression was determined by
582 fluorescence-activated flow cytometry analysis. The infectivity of pseudotyped
583 particles incubated with sybodies was compared with the infectivity observed using
584 pseudotyped particles and Dulbecco's modified Eagle's medium-2% fetal calf serum
585 only and standardized to 100%.
586
587 Average and standard deviation (SD, n=3) were plotted for the IC_{50} experiments
588 except for Fig. 4D which reports data from two independent experiments.
589

590 **Crystallization**

591 Crystallization trials were set up using a Crystal Gryphon LCP robot as follows. To
592 a two-well sitting-drop plate, 70 μL of precipitant solution was added to the reservoir.
593 To each well, 150 nL of protein solution was added using the LCP arm of the robot. The
594 wells were covered with 150 nL of precipitant solution using the 96-headed tips. Plates
595 were sealed using a tape (Cat HR4-506, Hampton research) and placed at 20 °C in a
596 Rocker Imager 1000 for automatic imaging.
597
598 Crystals for the SR4-RBD complex were grown in 20% (w/v) PEG 3,000, 200 mM
599 sodium chloride, 100 mM HEPES pH 7.5. Cryo protection was achieved by adding
600 20 %(v/v) glycerol to the mother liquor condition. Crystals for the MR17-RBD complex
601 were grown in 20 %(w/v) PEG 3,350, 0.2 M magnesium formate. Cryo protection was
602 achieved by adding 10 %(v/v) glycerol in the mother liquor condition. Crystals for the
603 MR3-RBD complex were obtained in 9 %(w/v) PEG 8,000, 0.1 M HEPES pH 7.5, 8 %(v/v)
604 ethylene glycol, 9.6 %(v/v) glycerol. 20% glycerol was included for cryo cooling. Crystals
605 for the MR4-RBD complex were grown in 10 %(w/v) PEG 8,000, 200 mM zinc acetate,
606 100 mM MES pH 6.0. Crystals for MR17-K99Y were grown in 0.2 M $MgCl_2$, 20 %(w/v)

607 PEG 3,350. Cryo protection was performed by adding 30 %(v/v) glycerol to the
608 reservoir condition. Crystals were cryo-protected, harvested using a MitGen loop, and
609 flash-cooled in liquid nitrogen before X-ray diffraction data collection.
610

611 **Data collection and structure determination**

612 X-ray diffraction data were collected at beamline BL19U1 (ref.[45]) at Shanghai
613 Synchrotron Radiation Facility. Diffraction data were collected with a 50 x 50 µm beam
614 on a Pilatus detector at a distance of 300 – 500 mm, with oscillation of 0.5 - 1° and a
615 wavelength of 0.97853 Å. Data were integrated using XDS [46], and scaled and merged
616 using Aimless [47]. The structure was solved by molecular replacement using Phaser [48]
617 with the RBD structure from PDB 6M0J and the sybody from PDB 5M13 [26] as the search
618 model. The model was built with $2F_o$-F_c maps in Coot [49], and refined using Phenix [50].
619 Structures were visualized using PyMol [51].

620

621 **Structure-based design of sybody mutants to improve binding affinity**

622 The structure of the MR17-RBD complex was examined using Coot[49] and PyMol[51].
623 A panel of 19 single mutants was designed by virtual mutation using Coot [49] followed
624 by examining the possible increasing in numbers of H-bonds, salt bridges, or
625 hydrophobic interactions. The mutations include V31F, V31I, E35F, G47A, G47F, G47W,
626 E52F, E52M, E52Q, S53k, S53Q, H56F, H56I, H56W, H56Y, K99Y, Q103D, Q103E, and
627 Q103Y. The mutants were purified and characterized the same way as for MR17.
628 Because K99Y showed higher neutralization activity than the wild-type, K99W was
629 designed for the second round.

630

631 ***In vivo* stability of sybody in mice**

632 The female 7-week-old ICR mice weighing 27 ± 1 g were intraperitoneally injected
633 with phosphate buffered saline (PBS) or sybodies MR3, MR3-MR3, or MR3-MR3-ABD
634 at 25mg kg^{-1} in a final volume of 100 µL in PBS. The blood samples were collected at
635 different time points (2 days preinjection, 6 h, 12h, 1 day, 3 days, 6 days and 14 days
636 postinjection) and subjected to neutralization assay using SARS-CoV-2 pseudotypes.
637 Mice weights were measured till 6 days post-injection (n=4). Mice were sacrificed at 1,
638 3, and 6 days post-injection; their vital organs (heart, liver, spleen, lung, kidney and
639 thymus) were fixed in 4% formaldehyde at 4 °C overnight and then embedded within
640 paraffin, solidified and cut to 15-µm thickness using a cryotome (Leica Microsystems).
641 Sections were stained by hematoxylin and eosin. Scale is equal to the original

642 magnification ×100.

643

644 **Mice challenge experiments**

645 C57BL/6J female mice (6-8 weeks old) were treated with adenovirus serotype 5
646 expressing human angiotensin 1 converting enzyme 2 (hACE2) via the intranasal route
647 as previously described[40]. At 5 days post-adenovirus treatment, the mice were
648 intranasally infected with SARS-CoV-2 strain hCoV-19/China/CAS-B001/2020 (National
649 Microbiology Data Center *NMDCN0000102-3*, GISAID databases *EPI_ISL_514256-7*)
650 with a high dose of 5×10^6 $TCID_{50}$ in a volume of 50 μL. After 12 h, the mice of MR3-
651 MR3-ABD group (n=6) was given 200 μL of sybody each (25 mg kg^{-1} body weight) by
652 intraperitoneal injection. The infection control group (n=3) was treated with PBS buffer.
653 Three days post-infection (d.p.i), three mice were euthanized, and the lung tissues
654 (~1/8 of the total lungs) were fixed in 4 %(v/v) paraformaldehyde for histopathological
655 analysis using hematoxylin-eosin staining. The rest of the lungs were weighted and
656 homogenized for RNA extraction and virus titration by quantitative reverse
657 transcription PCR (qRT-PCR) using a kit (Mabsky Biotech Co., Ltd.) following
658 manufacturer protocols. Average and standard deviation of all three individual data
659 points were reported.

660

661 **Ethics Statement**

662 The animal experiments were approved by the Institutional Animal Care and Use
663 Committee of the Institut Pasteur of Shanghai, Chinese Academy of Sciences (Animal
664 protocol No. A2020009) for in vivo stability assays, and by the Ethics Committees of
665 Institute of Microbiology, Chinese Academy of Sciences (SQIMCAS2020010) for the live
666 virus-related work. The study was conducted in strict accordance with the
667 recommendations provided in the Guide for the Care and Use of Laboratory Animals
668 of the Ministry of Science and Technology of the People's Republic of China. All
669 experiments with live viruses and animals were performed in a biosafety level 3
670 laboratory and complied with the instructions of the institutional biosafety manual.

671

672 **Data availability**

673 The structure factors and coordinates are available through the protein data bank
674 (PDB) under accession codes 7C8V (SR4-RBD), 7C8W (MR17-RBD), and 7CAN (MR17-
675 K99Y in complex with the RBD).

676 **Table S1. Sequences and FSEC results of sybody binders for the SARS-CoV-2 RBD.**

Sybody	FSEC shift[a]	Sequence[b]
Concave		
SR1	Y	QVQLVESGGGLVQAGGSLRLSCAASGFPVAAYEMEWYRQAPGKEREWVAAINSMGDQTY YADSVKGRFTISRDNAKNTVYLQMNSLKPEDTAVYYCYVYVGFSYIGQGTQVTVS
SR2	N	QVQLVESGGGLVQAGGSLRLSCAASGFPVKQQEMTWYRQAPGKEREWVAAIESNGHGTEY ADSVKGRFTISRDNAKNTVYLQMNSLKPEDTAVYYCYVYVGQSYIGQGTQVTVS
SR3	N	QVQLVESGGGLVQAGGSLRLSCAASGFPVWQEEMEWYRQAPGKEREWVAAITSYGDTTYY ADSVKGRFTISRDNAKNTVYLQMNSLKPEDTAVYYCVVYVGGTYIGQGTQVTVS
SR4	Y	QVQLVESGGGLVQAGGSLRLSCAASGFPVYSWNMWWYRQAPGKEREWVAAIESHGDSTR YADSVKGRFTISRDNAKNTVYLQMNSLKPEDTAVYYCYVWVGHTYYGQGTQVTVS
SR5	Y	QVQLVESGGGLVQAGGSLRLRCAASGFPVETTEMEWYRQAPGKEREWVAAISSYGSETYYA DSVKGRFTISRDNAKNTVYLQMNSLKPEDTAVYYCYVYVGTSYLGQGTQVTVS
SR6	N	QVQLVESGGGLVQAGGSLRLSCAASGFPVGQQEMTWYRQAPGKEREWVAAILSEGNGTEY ADSVKGRFTISRDNAKNTVYLQMNSLKPEDTAVYYCAVYVGATYIGQGTQVTVS
SR7	Y	QVQLVESGGGLVQAGGSLRLSCAASGFPVWSNEMEWYRQAPGKEREWVAAITSYGTTEYA DSVKGRFTISRDNAKNTVYLQMNSLKPEDTAVYYCYVYVGYSYIGQGTQVTVS
SR8	N	QVQLVESGGGLVQAGGSLRLSCAASGFPVYKREMTWYRQAPGKEREWVAAISSKGVHTEYA DSVKGRFTISRDNAKNTVYLQMNSLKPEDTAVYYCYVYVGKSYIGQGTQVTVS
SR9	N	QVQLVESGGGLVQAGGSLRLSCAASGFPVIAYEMEWYRQAPGKEREWVAAITSSGTSTYYA DSVKGRFTISRDNAKNTVYLQMNSLKPEDTAVYYCYVYVGQSYLGQGTQVTVS
SR10	N	QVQLVESGGGLVQAGGSLRLSCAASGFPVNKREMTWYRQAPGKEREWVAAITSEGRSTEYA DSVKGRFTISRDNAKNTVYLQMNSLKPEDTAVYYCYVFVGSSYIGQGTQVTVS
SR11	N	QVQLVESGGGLVQAGGSLRLSCAASGFPVYSMEMEWYRQAPGKEREWVAAISSWGNETH YADSVKGRFTISRDNAKNTVYLQMNSLKPEDTAVYYCYVYVGASYIGQGTQVTVS
SR12	N	QVQLVESGGGLVQAGGSLRLSCAASGFPVNMQEMEWYRQAPGKEREWVAAISSTGWVTY YADSVKGRFTISRDNAKNTVYLQMNSLKPEDTAVYYCYVYVGASYIGQGTQVTVS
SR13	Y	QVQLVESGGGLVQAGGSLRLSCAASGFPVDYMEMEWFRQAPGKEREWVAAITSNGRETYY ADSVKGRFTVSRDNAKNTVYLQMNSLKPEDTAVYYCYVYVGSSYIGQGTQVTVS
SR14	N	QVQLVESGGGLVQAGGSLRLSCAASGFPVDSEEMTWYRQAPGKEREWVAAITSDGDITEYA DSVKGRFTISRDNAKNTVYLQMNSLKPEDTAVYYCYVWVGRSYLGQGTQVTVS
SR15	N	QVQLVESGGGLVQAGGSLRLSCAASGFPVKHAEMEWYRQAPGKEREWVAAISSNGSETYY ADSVKGRFTISRDNAKNTVYLQMNSLKPEDTAVYYCYVWVGQSYIGQGTQVTVS
SR16	N	QVQLVESGGGLVQAGGSLRLSCAASGFPVKKYEMTWYRQAPGKEREWVAAITSKGTYTYYA DSVKGRFTISRDNAKNTVYLQMNSLKPEDTAVYYCYVYVGYSYLGQGTQVTVS
SR17	N	QVQLVESGGGLVQAGGSLRLSCAASGFPVEGSEMEWYRQAPGKEREWVAAIESNGTHTHY ADSVKGRFTISRDNAKNTVYLQMNSLKPEDTAVYYCYVYVGAGYIGQGTQVTVS
SR18	Y	QVQLVESGGGLVQAGGSLRLSCAASGFPVWFQEMEWYRQAPGKEREWVAAISSQGTHTY YADSVKGRFTISRDNAKNTVYLQMNSLKPEDTAVYYCYVYVGASYLGQGTQVTVS
SR19	N	QVQLVESGGGLVQAGGSLRLSCAASGFPVNTMEMEWYRQAPGKEREWVAAINSSGQETY YADSVKGRFTISRDNAKNTVYLQMNSLKPEDTAVYYCYVYVGQSYIGQGTQVTVS
SR20	N	QVQLVESGGGLVQAGGSLRLSCAASGFPVTSYEMEWYRQAPGKEREWVAAIASWGYHTYY ADSVKGRFTISRDNAKNTVYLQMNSLKPEDTAVYYCYVYVGGSYIGQGTQVTVS
SR21	N	QVQLVESGGGLVQAGGSLRLSCAASGFPVSKTEMEWYRQAPGKEREWVAAIASAGAETYYA DSVKGRFTISRDNAKNTVYLQMNSLKPEDTAVYYCYVYVGQSYIGQGTQVTVS
SR22	N	QVQLVESGGGLVQAGGSLRLSCAASGFPVASHEMEWYRQAPGKEREWVAAIASSGQWTYY

		ADSVKGRFTISRDNAKNTVYLQMNSLKPEDTAVYYCYVYVGQSYIGQGTQVTVS
SR23	N	QVQLVESGGGLVQAGGSLRLSCAASGFPVYTSEMEWYRQAPGKEREWVAAIASTGAETAYA DSVKGRFTISRDNAKNTVYLQMNSLKPEDTAVYYCYVYVGRSYIGQGTQVTVS
SR24	N	QVQLVESGGGLVQAGGSLRLSCAASGFPVNAMEMTWYRQAPGKEREWVAAIMSEGTWT EYADSVKGRFTISRDNAKNTVYLQMNSLKPEDTAVYYCYVYVGASYIGQGTQVTVS
SR25	N	QVQLVESGGGLVQAGGSLRLSCAASGFPVNTAEMVWYRQAPGKEREWVAAIYSEGPITEYA DSVKGRFTISRDNAKNTVYLQMNSLKPEDTAVYYCYVYVGSSYIGQGTQVTVS
SR26	N	QVQLVESGGGLVQAGGSLRLSCAASGFPVNTREMEWYRQAPGKEREWVAAISSNGHKTYY ADSVKGRFTISRDNAKNTVYLQMNSLKPEDTAVYYCYVYVGRSYIGQGTQVTVS
SR27	N	QVQLVESGGGLVQAGGSLRLSCAASGFPVWEAEMEWYRQAPGKEREWVAAISSIGTSTAYA DSVKGRFTISRDNAKNTVYLQMNSLKPEDTAVYYCIVYVGKTYIGQGTQVTVS
SR28	N	QVQLVESGGGLVQAGGSLRLSCAASGFPVKMAEMEWYRQAPGKEREWVAAIQSAGRETYY ADSVKGRFTISRDNAKNTVYLQMNSLKPEDTAVYYCYVYVGAGYIGQGTQVTVS
SR29	N	QVQLVESGGGLVQAGGSLRLSCAASGFPVSQREMTWYRQAPGKEREWVAAIESEGEQTEY ADSVKGRFTISRDNAKNTVYLQMNSLKPEDTAVYYCYVYVGRSYIGQGTQVTVS
SR30	N	QVQLVESGGGLVQAGGSLRLSCAASGFPVRKHEMEWYRQAPGKEREWVAAISSKGSNTYY ADSVKGRFTISRDNAKNTVYLQMNSLKPEDTAVYYCYVYVGASYIGQGTQVTVS
SR31	Y	QVQLVESGGGLVQAGGSLRLSCAASGFPVWQGEMAWYRQAPGKEREWVAAISSMGYKTY YADSVKGRFTISRDNAKNTVYLQMNSLKPEDTAVYYCAVMVGFWYAGQGTQVTVS
SR32	N.D.	QVQLVESGGGLVQAGGSLRLSCAASGFPVNVAKMAWYRQAPGKEREWVAAIDSHGAQTH YADSVKGRFTISRDNAKNTVYLQMNSLKPEDTAVYYCAVHVGFWYAGQGTQVTVS
SR33	N	QVQLVESGGGLVQAGGSLRLSCAASGFPVGSNEMEWYRQAPGKEREWVAAIQSSGVFTYY ADSVKGRFTISRDNAKNTVYLQMNSLKPEDTAVYYCYVYVGGSYLGQGTQVTVS
SR34	Y	QVQLVESGGGLVQAGGSLRLSCAAGGFPVKDHEMEWYRQAPGKEREWVAAITSSGWGTN TYYADSVKGRFTISRDNAKNTVYLQMNSLKPEDTAVYYCYVYVGSSYIGQGTQVTVS
SR35	N	QVQLVESGGGLVQAGGSLRLSCAASGFPVKHQTMEWYRQAPGKEREWVAAIMSKGRKTEY ADSVKGRFTISRDNAKNTVYLQMNSLKPEDTAVYHCHVYVGATYFGQGTQVTVS
SR36	N	QVQLVESGGGLVQAGGSLRLSCAASGFPVYMEEMEWYRQAPGKEREWVAAIASYGSETYY ADSVKGRFTISRDNAKNTVYLQMNSLKPEDTAVYYCYVYVGQSYIGQGTQVTVS
SR37	N	QVQLVESGGGLVQAGGSLRLSCAASGFPVSTAEMTWYRQAPGKEREWVAAIESYGNSTEYA DSVKGRFTISRDNAKNTVYLQMNSLKPEDTAVYYCYVYVGYSYIGQGTQVTVS
SR38	Y	QVQLVESGGGLVQAGGSLRLSCAASGFPVNQEEMEWYRQAPGKEREWVAAIKSWGTLTAY ADSVKGRFTISRDNAKNTVYLQMNSLKPEDTAVYYCAVHVGQTYIGQGTQVTVS
SR39	N	QVQLVESGGGLVQAGGSLRLSCAASGFPVDASEMEWYRQAPGKEREWVAAIESQGYETYY ADSVKGRFTISRDNAKNTVYLQMNSLKPEDTAVYYCYVYVGSSYIGQGTQVTVS
SR40	N	QVQLVESGGGLVQAGGSLRLSCAASGFPVDSQEMEWYRQAPGKEREWVAAISSNGKSTYY ADSVKGRFTISRDNAKNTVYLQMNSLKPEDTAVYYCYVYVGLSYIGQGTQVTVS
SR41	N	QVQLVESGGGLVQAGGSLRLSCAASGFPVGSTEMEWYRQAPGKEREWVAAISSTGHYTHYA DSVKGRFTISRDNAKNTVYLQMNSLKPEDTAVYYCYVYVGGSYLGQGTQVTVS
SR42	N	QVQLVESGGGLVQAGGSLRLSCAASGFPVQQREMTWYRQAPGKEREWVAAIMSKGVHTE YADSVKGRFTISRDNAKNTVYLQMNSLKPEDTAVYYCHVYVGASYFGQGTQVTVS
SR43	N.D.	QVQLVESGGGLVQAGGSLRLSCAASGFPVKKHEMEWYRQAPGKEREWVAAIQSKGYTTYY ADSVKGRFTISRDNAKNTVYLQMNSLKPEDTAVYYCYVYVGESYIGQGTQVTVS
SR44	N.D.	QVQLVESGGGLVQAGGSLRLSCAASGFPVGTAQMAWYRQAPGKEREWVAAITSYGEYTLYA DSVKGRFTISRDNAKNTVYLQMNSLKPEDTAVYYCAVHVGFWYTGQGTQVTVS
SR45	N.D.	QVQLVESGGGLVQAGGSLRLSCAASGFPVDNATMAWYRQAPGKEREWVAAIHSIGGYTTY ADSVKGRFTISRDNAKNTVYLQMNSLKPEDTAVYYCVGVGKHYYGQGTQVTVS

SR46	N.D.	QVQLVESGGGLVQAGGSLRLSCAASGFPVFTENMHWYRQAPGKEREWVAAIYSYGVWTLY ADSVKGRFTISRDNAKNTVYLQMNSLKPEDTAVYYCVVQVGEWYEGQGTQVTVS
SR47	N.D.	QVQLVESGGGLVQAGGSLRLSCAASGFPVKTETMHWYRQAPGKEREWVAAIYSYGTYTLYA DSVKGRFTISRDNAKNTVYLQMNSLKPEDTAVYYCEVQVGEWYEGQGTQVTVS
SR48	N.D.	QVQLVESGGGLVQAGGSLRLSCAASGFPVNQNNMHWYRQAPGKEREWVAAIYSSGDFTLY ADSVKGRFTISRDNAKNTVYLQMNSLKPEDTAVYYCEVQVGFWYTGQGTQVTVS
SR49	N.D.	QVQLVESGGGLVQAGGSLRLSCAASGFPVFHAYMAWYRQAPGKEREWVAAIESDGSSTHY ADSVKGRFTISRDNAKNTVYLQMNSLKPEDTSVYYCAVLVGFWYAGQGTQVTVS
SR50	N.D.	QVQLVESGGGLVQAGGSLRLNCAASGFPVAQAVMAWYRQALGKEREWVAAMHSTGTYTA YADSVKGRFTISRDNAKNTVYLQMNSLKPEDTAVYYCAVHVGFWYAGQGTQVTVS
SR51	N.D.	QVQLVESGGGLVQAGGSLRLSCAASGFPVWESYMRWYRQAPGKEREWVAAIQSNGNNT WYADSVKGRFTISRDNAKNTVYLQMNSLKPEDTAVYYCVVYVGYEYHGQGTQVTVS
SR52	N.D.	QVQLVESGGGLVQAGGSLRLSCAASGFPVNNMEMTWYRQAPGKEREWVAAIASDGSYTE YADSVKGRFTISRDNAKNTVYLQMNSLKPEDTAVYYCYVWVGKSYIGQGTQVTVS
SR53	N.D.	QVQLVESGGGLVQAGGSLRLSCAASGFPVYSQHMHWYRQAPGKEREWVAAIYSNGTYTLY ADSVKGRFTISRDNAKNTVYLQMNSLKPEDTAVYYCEVNVGEWYEGQGTQVTVS
SR54	N.D.	QVQLVESGGGLVQAGGSLRLSCAASGFPVSQARMHWYRQAPGKEREWVAAIGSSGDFTRY ADSVKGRFTISRDNAKNTVYLQMNSLKPEDTAVYYCEVQVGQWYEGQGTQVTVS
SR55	N.D.	QVQLVESGGGLVQAGGSLRLSCAASGFPVDTTNMHWYRQAPGKEREWVAAIYSSGGFTLY ADSVKGRFTISRDNAKNTVYLQMNSLKPEDTAVYYCTVWVGDWYEGQGTQVTVS
SR56	N.D.	QVQLVESGGGLVQAGGSLSLSCAASGFPVEHYGMYWYRQAPGKEREWVAAIRSDGQWTH YADSVKGRFTISRDNAKNTVYLQMNSLKPEDTAVYYCTVGVGSNYYGQGTQVTVS
SR57	N.D.	QVQLVESGGGLVQAGGSLRLSCAASGFPVEQAEMAWYRQAPGKEREWVAAIVSYGHSTYY ADSVKGRFTISRDNAKNTVYLQMNSLKPEDTAVYYCAVFVGFWYAGQGTQVTVS
SR58	N.D.	QVQLVESGGGLVQAGGSLRLSCAASGFPVKQENMHWYRQAPGKEREWVAAIYSTGNFTLY ADSVKGRFTISRDNAKNTVYLQMNSLKPEDTAVYYCAVQVGQWYEGQGTQVTVS
SR59	N.D.	QVQLVESGGGLVQAGGSLRLSCAASGFPVKTSRMYWYRQAPGKEREWVAAIISYGSVTFYA DSVKGRFTISRDNAKNTVYLQMNSLKPEDTAVYYCYVYVGAQYWGQGTQVTVS
SR60	N.D.	QVQLVESGGGLVQAGGSLRLSCAASGFPVEHAQMAWYRQAPGKEREWVAAIQSYGSTTYY ADSVKGRFTISRDNAKNTVYLQMNSLKPEDTAVYYCAVHVGFWYAGQGTQVTVS
SR61	N.D.	QVQLVESGGGLVQAGGSLRLSCAASGFPVDIAEMAWYRQAPGKEREWVAAIGSQGMTTH YADSVKGRFTISRDNAKNTVYLQMNSLKPEDTAVYYCAVHVGFWYAGQGTQVTVS
SR62	N.D.	QVQLVESGGGLVQAGGSLRLSCAASGFPVFQENMHWYRQAPGKEREWVAAIYSQGSYTLY ADSVKGRFTISRDNAKNTVYLQMNSLKPEDTAVYYCEVNVGQWYYGQGTQVTVS

Loop

MR1	N	QVQLVESGGGLVQVGGSLRLSCAASGFPVYHSIMHWYRQAPGKEREWVAAIYSSGAHTYYA DSVKGRFTISRDNAKNTVYLQMNSLKPEDTAVYYCNVKDGGNWDHTYDYWGQGTQVTVS
MR2	Y	QVQLVESGGGLVQAGGSLRLSCAASGFPVYFSYMAWYRQAPGKEREWVAAINSEGDSTTYA DSVKGRFTISRDNAKNTVYLQMNSLKPEDTAVYYCNVKDYGWYNSQYDYWGQGTQVTVS
MR3	Y	QVQLVESGGGLVQAGGSLRLSCAASGFPVNAHFMYWYRQAPGKEREWVAAIYSYGRTLYA DSVKGRFTISRDNAKNTVYLQMNSLKPEDTAVY YCNVKDYGAASWEYDYWGQGTQVTVS
MR4	Y	QVQLVESGGGLVQAGGSLRLSCAASGFPMYAWEMAWYRQAPGKEREWVAAIRSMGVHT HYSDSVKGRFTISRDNAKNTVYLQMNSLKPEDTAVYYCNVKDFGGHQAYYDYWGQGTQVT VS
MR5	N	QVQLVESGGGLVQAGGSLRLSCAASGFPVDAWEMAWYRQAPGKEREWVAAIRSFGRRTH YADSVKGRFTISRDNAKNTVYLQMNSLKPEDTAVYYCNVKDFGTHTQEYDYWGQGTQVTVS

MR6	Y	QVQLVESGGGLVQAGGSLRLSCAASGFPVEDTWMEWYRQAPGKEREWVAAITSWGFKTYYADSVKGRFTISRDNAKNTVYLQMNSLKPEDTAVYYCNVKDEGDTSASYDYWGQGTQVTVS
MR7	Y	QVQLVESGGGLVQAGGSLRLSCAASGFPVNSWMEWYRQAPGKEREWVAAITSYGYKTYYADSVKGRFTISRDNAKNTVYLQMNSLKPEDTAVYYCNVKDEGYFSDEYDYWGQGTQVTVS
MR8	Y	QVQLVESGGGLVQAGGSLRLSCAASGFPVEWAHMHWYRQAPGKEREWVAAIVSAGHYTVYADSVKGRFTISRDNAKNTVYLQMNSLKPEDTAVYYCNVKDWGSSNQYYDYWGQGTQVTVS
MR9	N	QVQLVESGGGLVQAGGSLRLSCAASGFPVASTWMEWYRQAPGKEREWVAAITSYGYHTYYADSVKGRFTISRDNAKNTVYLQMNSLKPEDTAVYYCNVKDEGYFSTNYDYWGQGTQVTVS
MR10	Y	QVQLVESGGGLVQAGGSLRLSCAASGFPVANTWMEWYRQAPGKEREWVAAITSYGYRTYYADSVKGRFTISRDNAKNTVYLQMNSLKPEDTAVYYCNVKDEGATTKVYDYWGQGTQVTVS
MR11	N.D.	QVQLVESGGGLVQAGGSLRLSCAASGFPVEWTSMVWYRQAPGKEREWVAAIYSAGHHTKYADSVKGRFTISRDNAKNTVYLQMNSLKPEDTAVYYCNVKDYGHDRSNYDYWGQGTQVTVS
MR12	N	QVQLVESGGGLVQAGGSLRLSCAASGFPVEWSHMHWYRQAPGKEREWVAAIVSTGEYTKYADSVKGRFTISRDNAKNTVYLQMNSLKPEDTAVYYCNVKDWYGQAKSYDYWGQGTQVTVS
MR13	N	QVQLVESGGGLVQAGGSLRLSCAASGFPVKNMNMHWYRQAPGKEREWVAAIYSYGVETHYADSVKGRFTISRDNAKNTVYLQMNSLKPEDTAVYYCNVKDWGSYMNWYDYWGQGTQVTVS
MR14	Y	QVQLVESGGGLVQAGGSLRLSCAASGFPVMYTHMHWYRQAPGKEREWVAAIVSLGEYTTYADSVKGRFTISRDNAKNTVYLQMNSLKPEDTAVYYCNVKDWGAANKYYDYWGQGTQVTVS
MR15	N	QVQLVESGGGLVQAGGSLRLSCAASGFPVDTWMEWYRQAPGKEREWVAAITSYGYKTYYADSVKGRFTISRDNAKNTVYLQMNSLKPEDTAVYYCNVKDFGYASTYYDYWGQGTQVTVS
MR16	N	QVQLVESGGGLVQAGGSLRLSCAASGFPVERTWMEWYRQAPGKEREWVAAITSYGYRTYYADSVKGRFTISRDNAKNTVYLQMNSLKPEDTAVYYCNVKDEGSASSAYDYWGQGTQVTVS
MR17	Y	QVQLVESGGGLVQAGGSLRLSCAASGFPVEVWRMEWYRQAPGKEREGVAAIESYGHGTRYADSVKGRFTISRDNAKNTVYLQMNSLKPEDTAVYYCNVKDDGQLAYHYDYWGQGTQVTVS
MR18	N	QVQLVESGGGLVQAGGSLRLSCAASGFPVWEHHMAWYRQAPGKEREWVAAITSKGRYTTYADSVKGRFTISRDNAKNTVYLQMNSLKPEDTAVYYCHVKDAGYFDAQYDYWGQGTQVTVS
MR19	N	QVQLVESGGGLVQAGGSLRLSCAASGFPVRNTEHMYWYRQAPGKEREWVAAIFSMGRFTKYADSVKGRFTISRDNAKNTVYLQMNSLKPEDTAVYYCNVKDTGSFSEGYDYWGQGTQVTVS

Convex

LR1	Y	QVQLVESGGGSVQAGGSLRLSCAASGSISSITYLGWFRQAPGKEREGVAALITDSGRTYYADSVKGRFTVSLDNAKNTVYLQMNSLKPEDTALYYCAAAEWGYEWPLYYASSWYWGQGTQVTVS
LR2	Y	QVQLVESGGGSVQAGGSLRLSCAASGDINAIGYLGWFRQAPGKEREGVAALDTDEGQTYYADSVKGRFTVSLDNAKNTVYLQMNSLKPEDTALYYCAAAMNGYNEPLYSYDYEYWGQGTQVTVS
LR3	Y	QVQLVESGGGSVQAGGSLRLSCAASGTINNITYLGWFRQAPGKEREGVAALITTSGYTYYADSVKGRFTVSLDNAKNTVYLQMNSLKPEDTALYYCAAASWGYEWPLVYDDYWYWGQGTQVTVS
LR4	N	QVQLVESGGGSVQAGGSLRLSCAASGFIHSIYYLGWFRQAPGKEREGVAALNTQHGTTYYADSVKGRFTVSLDNAKNTVYLQMNSLKPEDTALYYCAAARWGRNYPLNYWQYSYWGQGTQVTVS
LR5	Y	QVQLVESGGGSVQAGGSLRLSCAASGSISSITYLGWFRQAPGKEREGVAALITSNGRTYYADSVKGRFTVSLDNAKNTVYLQMNSLKPEDTALYYCAAATWGYHWPLGAWDYWYWGQGTQVTVS
LR6	Y	QVQLVESGGGSVQAGGSLRLSCAASGSISSITYLGWFRQAPGKEREGVAALVTTSGNTYYADS

		VKGRFTVSLDNAKNTVYLQMNSLKPEDTALYYCAAATWGYSWPLEHDEYWYWGQGTQVTVS
LR7	Y	QVQLVESGGGSVQAGGSLRLSCAASGSISSITYLGWFRQAPGKEREGVAALITNWGHTYYADSVKGRFTVSLDNAKNTVYLQMNSLKPEDTALYYCAAAFHGEQYPLYTNKYHYWGQGTQVTVS
LR8	Y	QVQLVESGGGSVQAGGSLRLSCAASGTIAYIKYLGWFRQAPGKEREGVAALMTRWGETYYADSVKGRFTVSLDNAKNTVYLQMNSLKPEDTALYYCAAANYGANFPLQANTYFYWGQGTQVTVS
LR9	N	QVQLVESGGGSVQAGGSLRLSCAASGSISSITYLGWFRQAPGKEREGVAALITARGRTYYADSVKGRFTVSLDNAKNTVYLQMNSLKPEDTALYYCAAANWGYNWPLAYSDYWYWGQGTQVTVS
LR10	N	QVQLVESGGGSVQAGGSLRLSCAASGTISSITYLGWFRQAPGKEREGVAALTTNNGHTYYADSVKGRFTVSLDNAKNTVYLQMNSLKPEDTALYYCAAADWGYDWPLDRYHYWYWGQGTQVTVS
LR11	Y	QVQLVESGGGSVQAGGSLRLSCAASGSISSITYLGWFRQAPGKEREGVAALVTHSGSTYYADSVKGRFTVSLDNAKNTVYLQMNSLKPEDTALYYCAAAYWGWDWPLNSQDYWYWGQGTQVTVS
LR12	N	QVQLVESGGGSVQAGGSLRLSCAASGSIASIKYLGWFRQAPGKEREGVAALMTRWGETYYADSVKGRFTVSLDNAKNTVYLQMNSLKPEDTALYYCAAAECGANSPLHAKDYSYWGQGTQVTVS
LR13	N	QVQLVESGGGSVQAGGSLRLSCAASGSISSITYLGWFRQAPGKEREGVAALITHAGRTYYADSVKGRFTVSLDNAKNTVYLQMNSLKPEDTALYYCAAADWGWYWPLVIDHYEYWGQGTQVTVS
LR14	N	QVQLVESGGGSVQAGGSLRLSCAASGSIPGITYLGWFRQAPGKEREGVAALVTNSGHTYYADSVKGRFTVSLDNAKNTVYLQMNSLKPEDTALYYCAAADWGYQWPLDKAEYWYWGQGTQVTVS
LR15	Y	QVQLVESGGGSVQAGGSLRLSCAASGSISSITYLGWFRQAPGKEREGVAALKTASGQTYYADSVKGRFTVSLDNAKNTVYLQMNSLKPEDTALYYCAAADWGYNWPLIREEYEYWGQGTQVTVS
LR16	Y	QVQLVESGGGSVQAGGSLRLSCAASGSISSITYLGWFRQAPGKEREGVAALYTTHGYTYYADSVKGRFTVSLDNAKNTVYLQMNSLKPEDTALYYCAAADWGYNIPLNITDYWYWGQGTQVTVS
LR17	N	QVQLVESGGGSVQAGGSLRLSCAASGSIAHIKYLGWFRQAPGKEREGVAALMTRHGQTYYADSVKGRFTVSLDNAKNTVYLQMNSLKPEDTALYYCAAAYYGANFPLFQTGYTYWGQGTQVTVS
LR18	N	QVQLVESGGGSVQAGGSLRLSCAASGSISSITYLGWFRQAPGKEREGVAALVTENGHTYYADSVKGRFTVSLDNAKNTVYLQMNSLKPEDTALYYCAAATWGYEWPLYSNDYFYWGQGTQVTVS

Divalent, bispecific

LR5-MR3 [13 GS]	QVQLVESGGGSVQAGGSLRLSCAASGSISSITYLGWFRQAPGKEREGVAALITSNGRTYYADSVKGRFTVSLDNAKNTVYLQMNSLKPEDTALYYCAAATWGYHWPLGAWDYWYWGQGTQVTVS*GGGGSGGGSGSSS*QVQLVESGGGLVQAGGSLRLSCAASGFPVNAHFMYWYRQAPGKEREWVAAIYSYGRTLYADSVKGRFTISRDNAKNTVYLQMNSLKPEDTAVYYCNVKDYGAASWEYDYWGQGTQVTVS
LR5-MR3 [19 GS]	QVQLVESGGGSVQAGGSLRLSCAASGSISSITYLGWFRQAPGKEREGVAALITSNGRTYYADSVKGRFTVSLDNAKNTVYLQMNSLKPEDTALYYCAAATWGYHWPLGAWDYWYWGQGTQVTVS*GGGGSGGGGSGGGGSGSSS*QVQLVESGGGLVQAGGSLRLSCAASGFPVNAHFMYWYRQAPGKEREWVAAIYSYGRTLYADSVKGRFTISRDNAKNTVYLQMNSLKPEDTAVYYCNVKD

	YGAASWEYDYWGQGTQVTVS
LR5-MR3 [34 GS]	QVQLVESGGGSVQAGGSLRLSCAASGSISSITYLGWFRQAPGKEREGVAALITSNGRTYYADS VKGRFTVSLDNAKNTVYLQMNSLKPEDTALYYCAAATWGYHWPLGAWDYWYWGQGTQV TVS*GGGGSGGGGSGGGGSGGGGSGGGGSGGGGSGSSS*QVQLVESGGGLVQAGGSLRLSC AASGFPVNAHFMYWYRQAPGKEREWVAAIYSYGRTLYADSVKGRFTISRDNAKNTVYLQM NSLKPEDTAVYYCNVKDYGAASWEYDYWGQGTQVTVS
Divalent, monospecific	
Fc-MR3	GSSS**QVQLVESGGGLVQAGGSLRLSCAASGFPVNAHFMYWYRQAPGKEREWVAAIYSYG RTLYADSVKGRFTISRDNAKNTVYLQMNSLKPEDTAVYYCNVKDYGAASWEYDYWGQGT QVTVS**ERKCCVECPPCPAPPVAGPSVFLFPPKPKDTLMISRTPEVTCVVVDVSHEDPEVQFN WYVDGVEVHNAKTKPREEQFNSTFRVVSVLTVVHQDWLNGKEYKCKVSNKGLPAPIEKTISK TKGQPREPQVYTLPPSREEMTKNQVSLTCLVKGFYPSDIAVEWESNGQPENNYKTTPPMLDS DGSFFLYSKLTVDKSRWQQGNVFSCSVMHEALHNHYTQKSLSLSPGK
MR3-MR3 [13 GS]	QVQLVESGGGLVQAGGSLRLSCAASGFPVNAHFMYWYRQAPGKEREWVAAIYSYGRTLYA DSVKGRFTISRDNAKNTVYLQMNSLKPEDTAVYYCNVKDYGAASWEYDYWGQGTQVTVS*G GGGSGGGSGSSS*QVQLVESGGGLVQAGGSLRLSCAASGFPVNAHFMYWYRQAPGKEREW VAAIYSYGRTLYADSVKGRFTISRDNAKNTVYLQMNSLKPEDTAVYYCNVKDYGAASWEYDY WGQGTQVTVS
MR3-MR3 [19 GS]	QVQLVESGGGLVQAGGSLRLSCAASGFPVNAHFMYWYRQAPGKEREWVAAIYSYGRTLYA DSVKGRFTISRDNAKNTVYLQMNSLKPEDTAVYYCNVKDYGAASWEYDYWGQGTQVTVS*G GGGSGGGGSGGGGSGSSS*QVQLVESGGGLVQAGGSLRLSCAASGFPVNAHFMYWYRQAP GKEREWVAAIYSYGRTLYADSVKGRFTISRDNAKNTVYLQMNSLKPEDTAVYYCNVKDYGAA SWEYDYWGQGTQVTVS
MR3-MR3 [24 GS]	QVQLVESGGGLVQAGGSLRLSCAASGFPVNAHFMYWYRQAPGKEREWVAAIYSYGRTLYA DSVKGRFTISRDNAKNTVYLQMNSLKPEDTAVYYCNVKDYGAASWEYDYWGQGTQVTVS*G GGGSGGGGSGGGGSGGGGSGSSS*QVQLVESGGGLVQAGGSLRLSCAASGFPVNAHFMY WYRQAPGKEREWVAAIYSYGRTLYADSVKGRFTISRDNAKNTVYLQMNSLKPEDTAVYYCNV KDYGAASWEYDYWGQGTQVTVS
MR3-MR3 [34 GS]	QVQLVESGGGLVQAGGSLRLSCAASGFPVNAHFMYWYRQAPGKEREWVAAIYSYGRTLYA DSVKGRFTISRDNAKNTVYLQMNSLKPEDTAVYYCNVKDYGAASWEYDYWGQGTQVTVS*G GGGSGGGGSGGGGSGGGGSGGGGSGGGGSGSSS*QVQLVESGGGLVQAGGSLRLSCAASG FPVNAHFMYWYRQAPGKEREWVAAIYSYGRTLYADSVKGRFTISRDNAKNTVYLQMNSLKP EDTAVYYCNVKDYGAASWEYDYWGQGTQVTVS
Fc-MR17	GSSS**QVQLVESGGGLVQAGGSLRLSCAASGFPVEVWRMEWYRQAPGKEREGVAAIESYG HGTRYADSVKGRFTISRDNAKNTVYLQMNSLKPEDTAVYYCNVKDDGQLAYHYDYWGQ GTQVTVS**ERKCCVECPPCPAPPVAGPSVFLFPPKPKDTLMISRTPEVTCVVVDVSHEDPEVQF NWYVDGVEVHNAKTKPREEQFNSTFRVVSVLTVVHQDWLNGKEYKCKVSNKGLPAPIEKTIS KTKGQPREPQVYTLPPSREEMTKNQVSLTCLVKGFYPSDIAVEWESNGQPENNYKTTPPMLD SDGSFFLYSKLTVDKSRWQQGNVFSCSVMHEALHNHYTQKSLSLSPGK
MR17m-MR17m (13 GS)	QVQLVESGGGLVQAGGSLRLSCAASGFPVEVWRMEWYRQAPGKEREGVAAIESYGHGTRY ADSVKGRFTISRDNAKNTVYLQMNSLKPEDTAVYYCNVYDDGQLAYHYDYWGQGTQVTVS *GGGGSGGGSGSSS*QVQLVESGGGLVQAGGSLRLSCAASGFPVEVWRMEWYRQAPGKERE GVAAIESYGHGTRYADSVKGRFTISRDNAKNTVYLQMNSLKPEDTAVYYCNVYDDGQLAYHY DYWGQGTQVTVS
MR17m-MR17m (16 GS)	QVQLVESGGGLVQAGGSLRLSCAASGFPVEVWRMEWYRQAPGKEREGVAAIESYGHGTRY ADSVKGRFTISRDNAKNTVYLQMNSLKPEDTAVYYCNVYDDGQLAYHYDYWGQGTQVTVS *GGGGSGGGGSGSGSSS*QVQLVESGGGLVQAGGSLRLSCAASGFPVEVWRMEWYRQAPGK EREGVAAIESYGHGTRYADSVKGRFTISRDNAKNTVYLQMNSLKPEDTAVYYCNVYDDGQLA

	YHYDYWGQGTQVTVS
MR17m-MR17m (19GS)	QVQLVESGGGLVQAGGSLRLSCAASGFPVEVWRMEWYRQAPGKEREGVAAIESYGHGTRYADSVKGRFTISRDNAKNTVYLQMNSLKPEDTAVYYCNVYDDGQLAYHYDYWGQGTQVTVS*GGGGSGGGGSGGGGSGSSS*QVQLVESGGGLVQAGGSLRLSCAASGFPVEVWRMEWYRQAPGKEREGVAAIESYGHGTRYADSVKGRFTISRDNAKNTVYLQMNSLKPEDTAVYYCNVYDDGQLAYHYDYWGQGTQVTVS
MR17m-MR17m (24 GS)	QVQLVESGGGLVQAGGSLRLSCAASGFPVEVWRMEWYRQAPGKEREGVAAIESYGHGTRYADSVKGRFTISRDNAKNTVYLQMNSLKPEDTAVYYCNVYDDGQLAYHYDYWGQGTQVTVS*GGGGSGGGGSGGGGSGGGGSGSSS*QVQLVESGGGLVQAGGSLRLSCAASGFPVEVWRMEWYRQAPGKEREGVAAIESYGHGTRYADSVKGRFTISRDNAKNTVYLQMNSLKPEDTAVYYCNVYDDGQLAYHYDYWGQGTQVTVS
ABD conjugation	
MR3-MR3-ABD	QVQLVESGGGLVQAGGSLRLSCAASGFPVNAHFMYWYRQAPGKEREWVAAIYSYGRTLYADSVKGRFTISRDNAKNTVYLQMNSLKPEDTAVYYCNVKDYGAASWEYDYWGQGTQVTVS*GGGGSGGGGSGGGGSGGGGSGGGGSGGGGSGSSS*QVQLVESGGGLVQAGGSLRLSCAASGFPVNAHFMYWYRQAPGKEREWVAAIYSYGRTLYADSVKGRFTISRDNAKNTVYLQMNSLKPEDTAVYYCNVKDYGAASWEYDYWGQGTQVTVSAGRA*GGGGGSGGGGSGGGGSG*TIDEWLLKEAKEKAIEELKKAGITSDYYFDLINKAKTVEGVNALKDEILKA

[a]Fluorescence-detection size exclusion chromatography (FSEC) assay for RBD binders. Periplasmic extraction was directly mixed with 0.5 μM of fluorescently labeled RBD and the mixture was loaded onto an analytic gel filtration column. Sybodies that caused earlier retention volume (peak shift) are labeled 'Y' and colored red. Sybodies that did not peak shift are indicated with 'N'. Sybodies that were not determined for FSEC peak-shift are labeled with 'N.D.'. [b]The sequences include 'GSSS' at the N-terminal, and 'AGRAG*EQKLISEEDL*NSAVDHHHHHH' at the C-terminal which contains a myc-tag (italic) for ELISA and a hexahistidine tag for purification. GS linker are highlighted in italic, when applicable.

Table S2. Data collection and refinement statistics.

	SR4-RBD	MR17-RBD	MR17(K99Y)-RBD
Data collection			
Space group	P 6_5 2 2	P3_2 2 1	P3_2 2 1
Cell dimensions			
a, *b*, *c* (Å)	65.55, 65.55, 344.53	73.69, 73.69, 158.58	74.19, 74.19, 158.40
α,*β*, *γ* (°)	90, 90, 120	90, 90, 120	90, 90, 120
Wavelength (Å)	0.97853	0. 97853	0.97853
Resolution (Å)	47.40 - 2.15	49.71 - 2.77	49.90 - 2.94
	(2.23 - 2.15)[a]	(2.89 - 2.77)	(3.12 - 2.94)
R_{merge}	0.161 (1.203)	0.276 (2.222)	0.218 (1.666)
R_{pim}	0.054 (0.395)	0.062 (0.494)	0.052 (0.385)
$I/\sigma I$	11.4 (2.0)	11.1 (1.5)	12.4 (1.9)
Completeness (%)	99.8 (99.9)	100 (99.9)	99.9 (99.6)
Multiplicity	9.5 (9.9)	21.0 (20.8)	18.4 (19.3)
*CC** [b]	0.999 (0.970)	0.997 (0.927)	0.998 (0.920)
Refinement			
Resolution (Å)	47.40 - 2.15	49.71 - 2.77	49.90 - 2.94
No. reflections	25,148	13,256	11,264
R_{work} / R_{free}	0.1836 / 0.2239	0.2029 / 0.2659	0.2149 / 0.2676
No. atoms	2,810	2,536	2,509
Protein	2,510	2,482	2,465
Ligands	62	54	44
Water	238	0	0
No. residues	322	315	312
B-factors (Å^2)	35.13	73.28	79.38
Protein	34.16	72.27	78.53
Ligand/ion	55.11	119.79	126.90
Water	40.22		
R.m.s deviations			
Bond lengths (Å)	0.007	0.011	0.004
Bond angles (°)	0.850	1.10	0.68
Ramachandran			
Favoured (%)	98.06	96.12	96.08
Allowed (%)	1.94	3.88	3.59
Outlier (%)	0	0	0.33
PDB ID	7C8V	7C8W	7CAN

[a]Highest resolution shell is shown in parenthesis. [b]$CC^* = \sqrt{\frac{2CC_{1/2}}{1+CC_{1/2}}}$

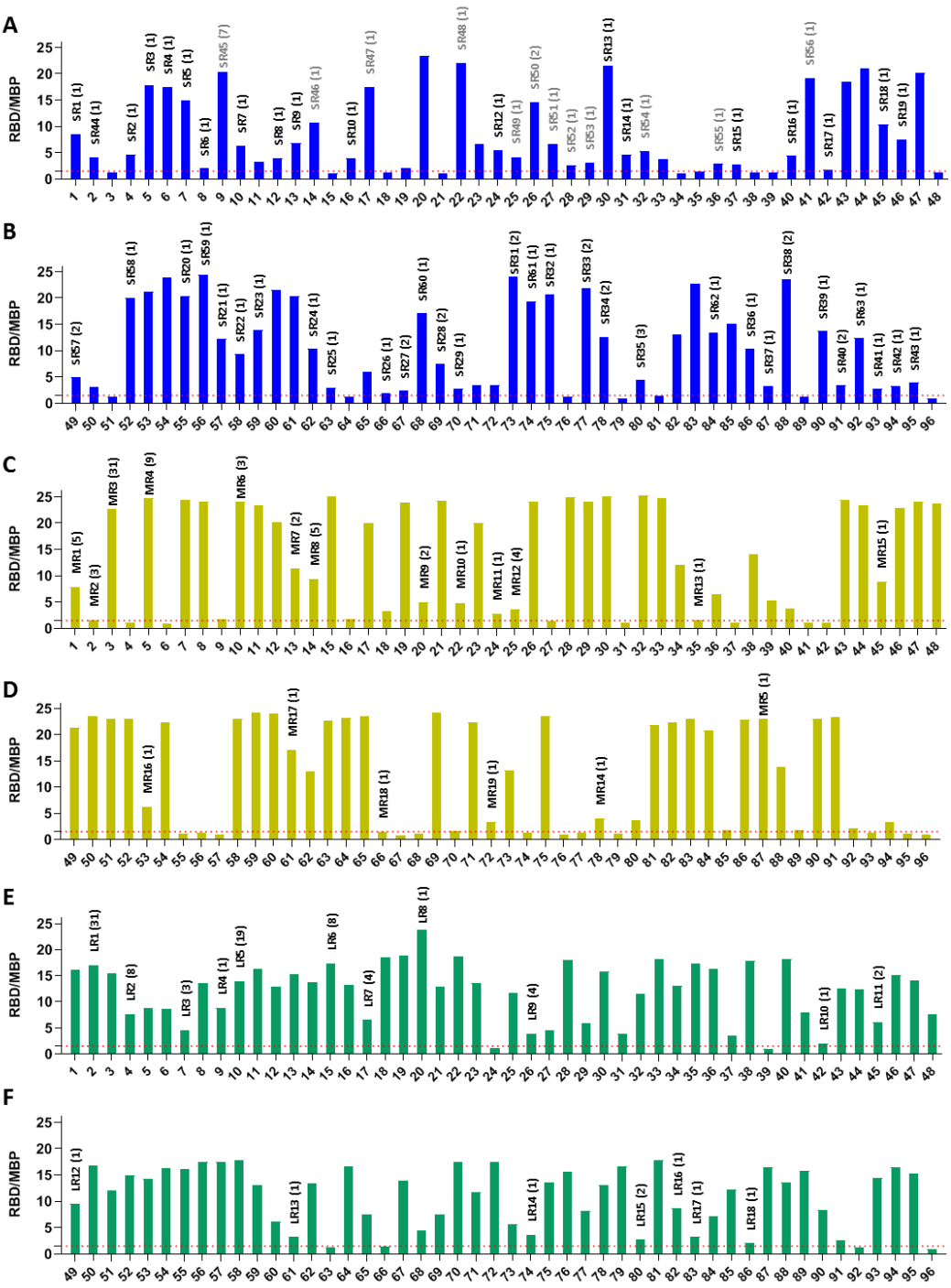

690

691 **Extended Data Fig. 1. Identification of RBD binders using ELISA.** (**A,B**) Results for the
692 Concave library. (**C,D**) Results for the Loop library. (**E,F**) Results for the Convex library.
693 The ratio between the ELISA signal (A_{650}) of wells with the RBD and of wells with the
694 unrelated maltose-binding protein (MBP) is plotted. The signal for MBP is typically
695 between 0.04-0.09. A red dashed line guides the cut-off at a ratio of 1.5. Unique
696 clones are labeled with the redundancy shown in brackets.

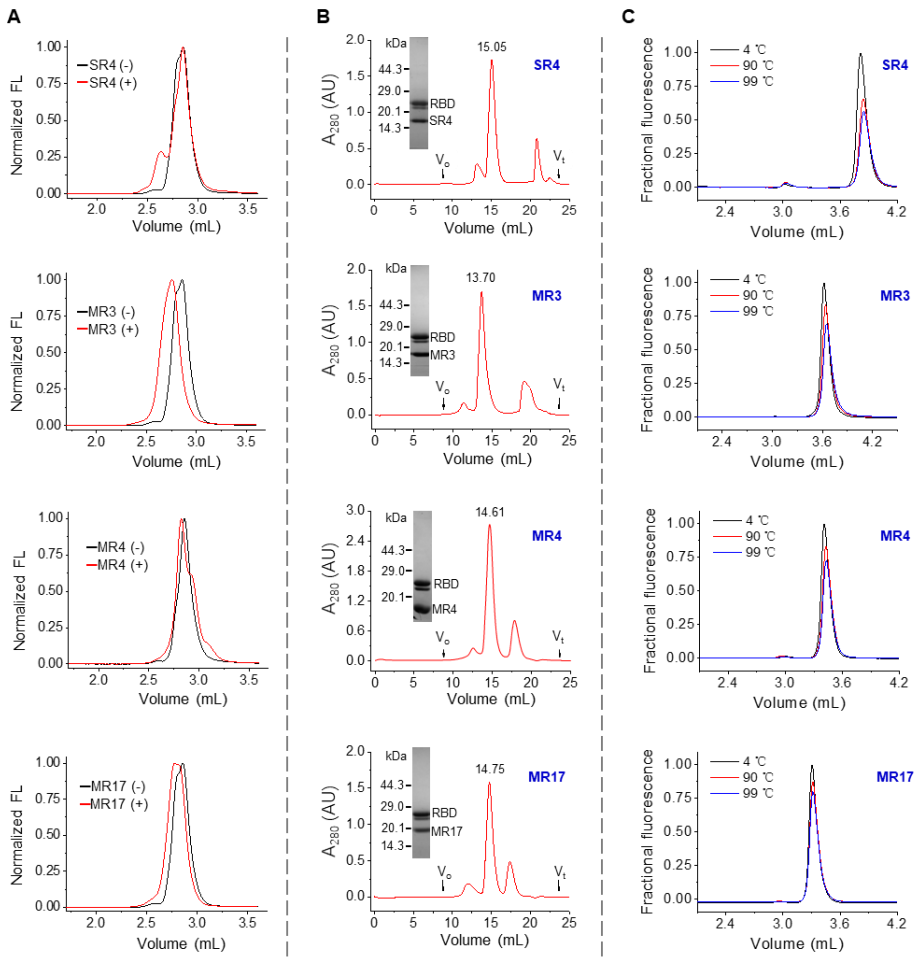

Extended Data Fig. 2. Characterization and purification of sybody-RBD complexes. (**A**) Fluorescence-detector size exclusion chromatography (FSEC) of the RBD in the absence (black, -) and presence (red, +) of crude periplasmic extract from sybody clones. Biotinylated RBD was fluorescently labeled through binding to streptavidin that was conjugated with an amine-reactive fluorescein variant. The concentration of RBD was 0.5 μM. Fluorescence (Ex. 482 nm, Em. 508 nm) was normalized before plotting. The extent of peak shift follows the order of SR4<MR4<MR17<MR3. Fluorescence trace before the void volume (V_o, 1.78 mL) is not shown. (**B**) Preparative size exclusion chromatography of the indicated sybody-RBD complexes. SDS-PAGE images of the main-peak fraction for all four sybodies are shown in the inset. Numbers label the elution volume for the main peak. The results for SR34, SR38, MR6, LR1, and LR5 were similar to the 4 sybodies here and are not shown. (**C**) Fluorescence-detection size exclusion chromatography (FSEC) profile of the thermostability assay. Sybodies SR4, MR17, MR3, and MR4 were incubated at indicated temperatures for 20 min before loading on to an analytical size exclusion chromatography column. The elution profile was monitored using the intrinsic tryptophan fluorescence. Fluorescence intensities were normalized to the peak value of the unheated sample.

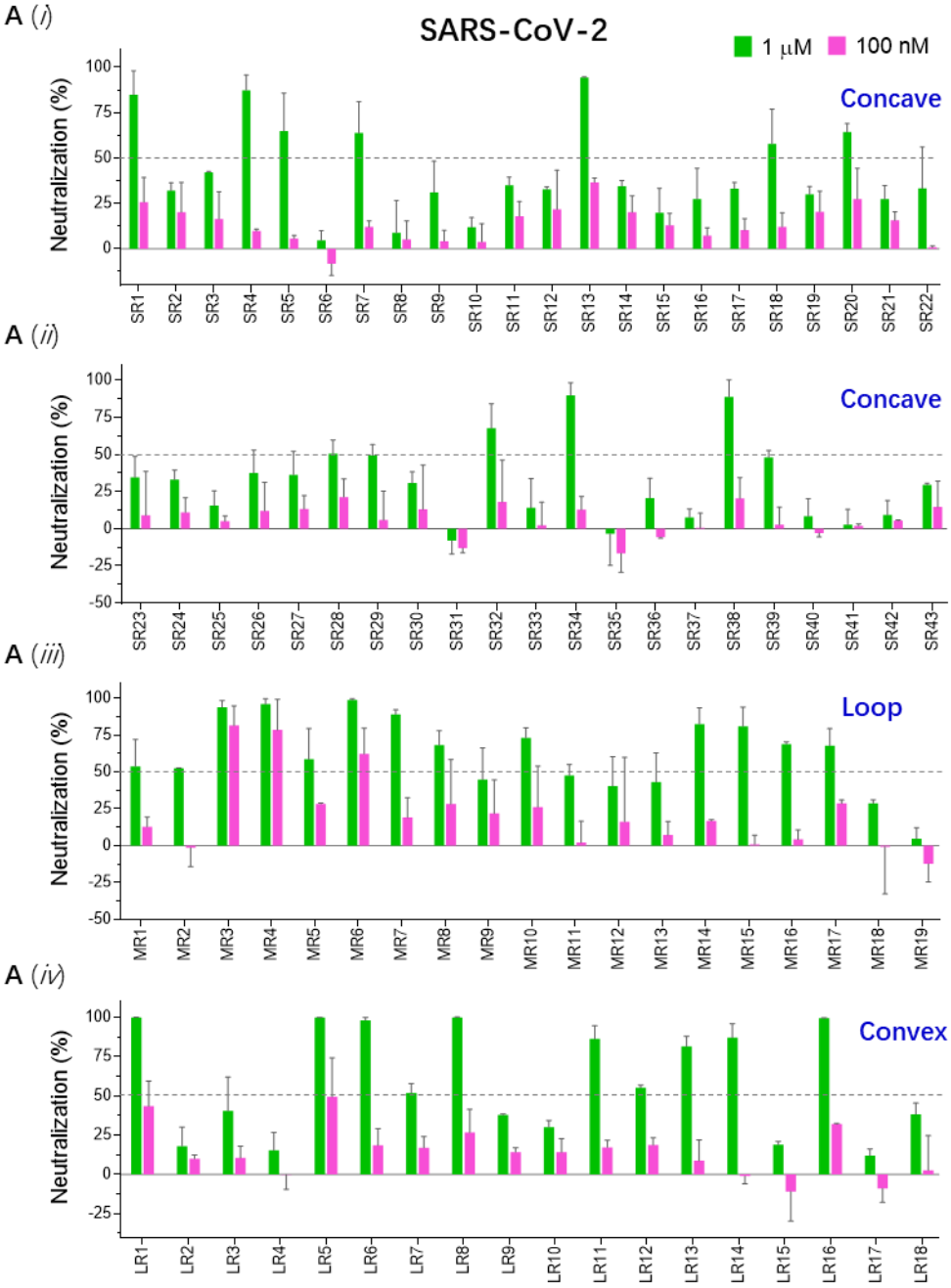

Extended Data Fig. 3 **- to be continued on the next page**

715

Extended Data Fig. 3 - continued from the previous page

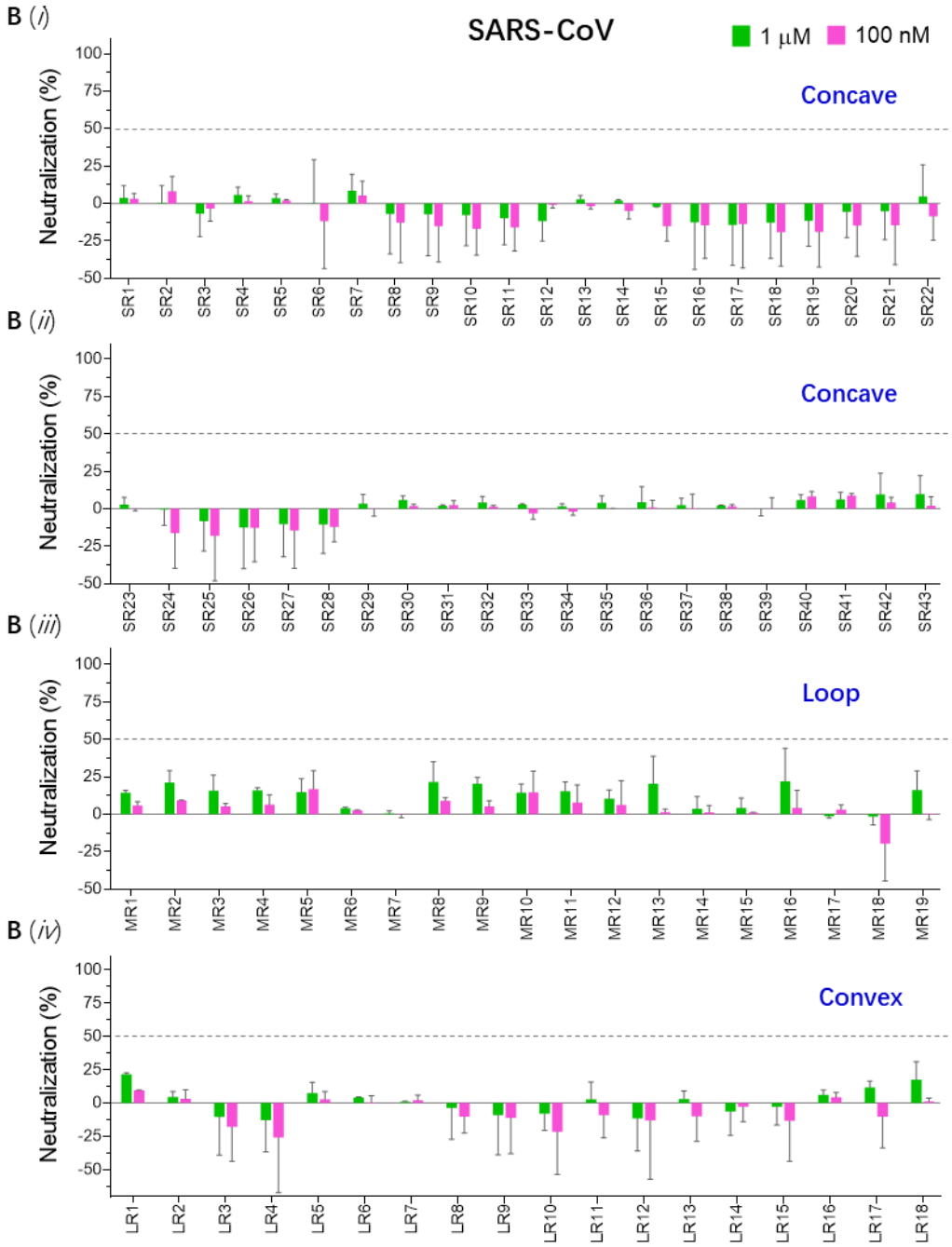

716

717

718 **Extended Data Fig. 3. Neutralization activity of 80 sybodies.** (**A**) Neutralization assay
719 results for SARS-CoV-2 pseudovirus. (**B**) Neutralization assay results for SARS-CoV
720 pseudovirus. VeroE6-hACE2 cells were infected with a premix of pseudotypes and
721 sybodies at two concentrations (1 μM and 100 nM). Infectivity were measured after 3
722 days using FACS and the percentage of neutralization was calculated for each sybody.

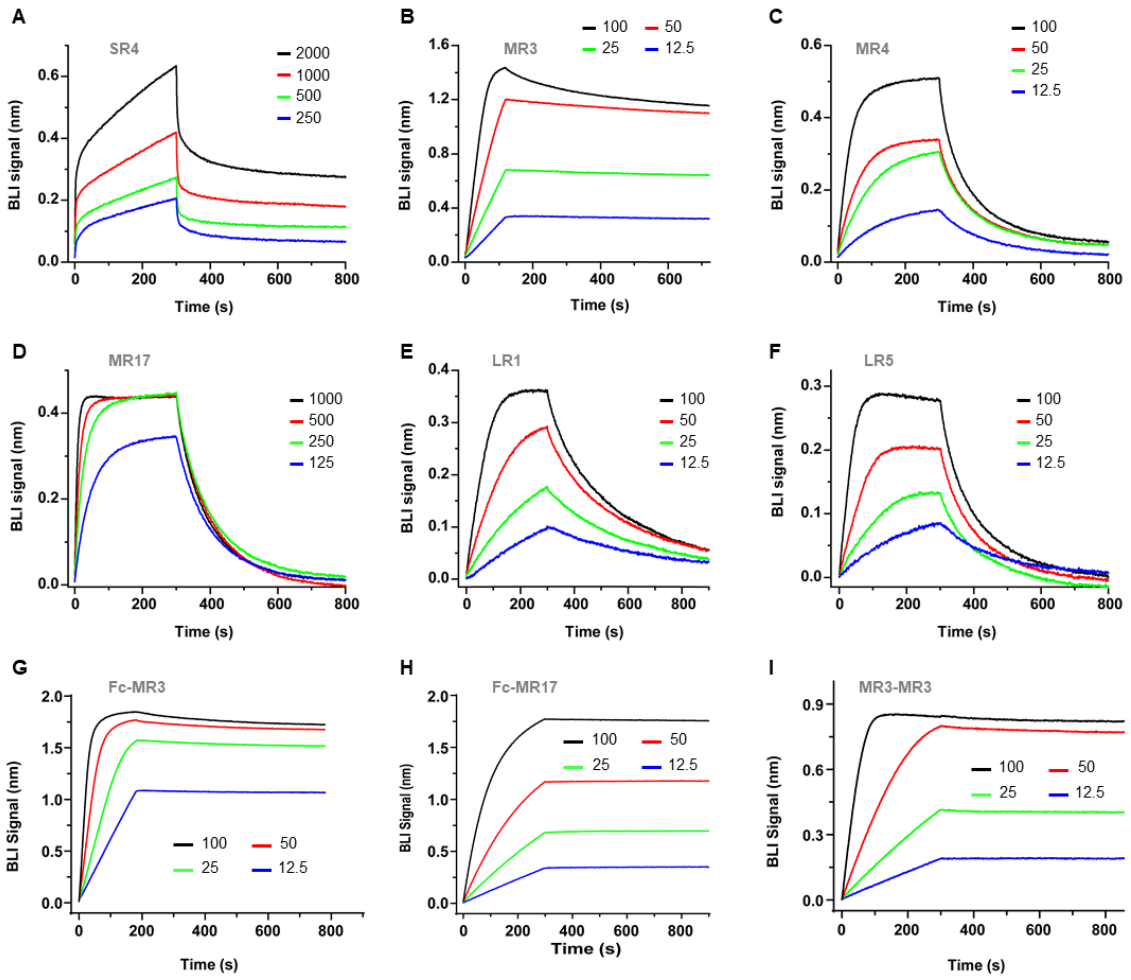

723

724 **Extended Data Fig. 4. Kinetics for sybody-RBD binding.** (**A-I**) Biotinylated RBD
725 immobilized on a streptavidin-coated sensor was titrated with various concentrations
726 (nM) of sybodies as indicated. Bio-layer interferometry (BLI) data were fitted with a 1:1
727 stoichiometry.

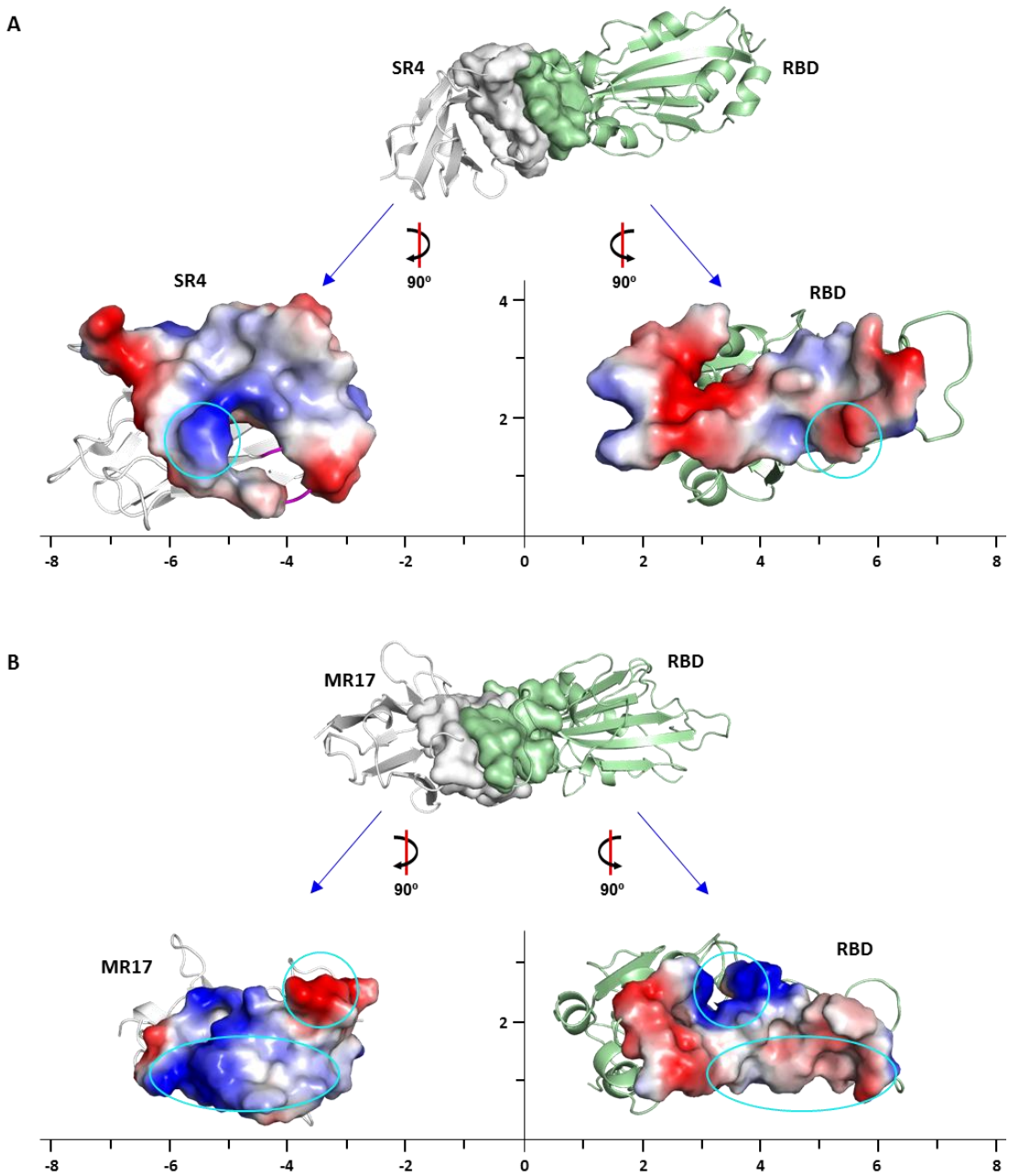

Extended Data Fig. 5. Electrostatic complementarity of the sybody-RBD binding surface. (**A,B**) 'Open-book' view of molecular electrical potential surfaces of the interface between the RBD and SR4 (**A**) and between the RBD and MR17 (**B**). The electrical potential maps were calculated by Adaptive Poisson-Boltzmann Solver (APBS) [52] built-in in PyMol. The unitless ruler guides the view of the relative distances between the opened surface pairs. Cyan circles highlight electrostatic complementarity.

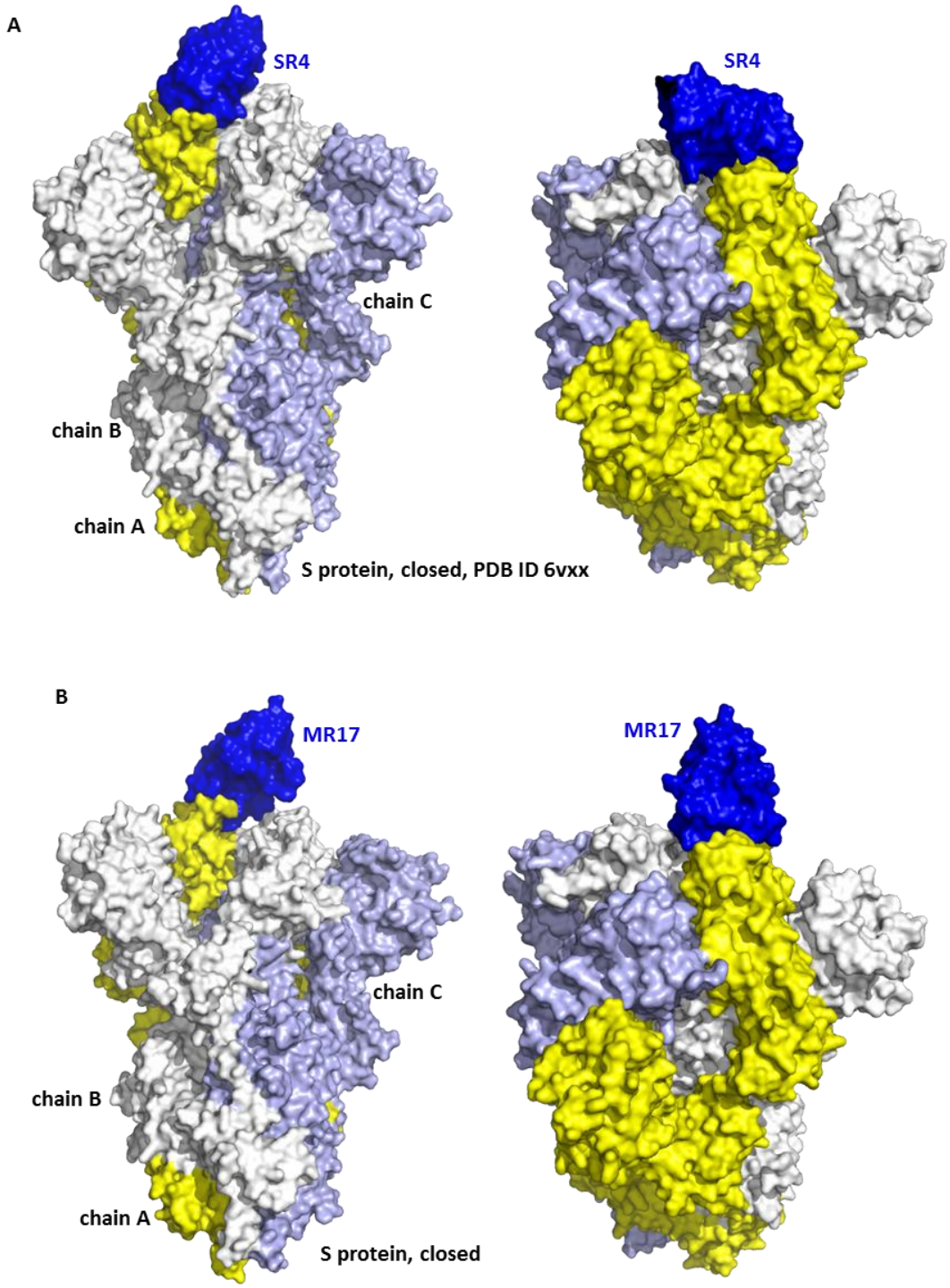

Extended Data Fig. 6. SR4 and MR17 may bind to the SARS-CoV-2 S RBD in the 'closed' conformation. (**A,B**) The structure of SR4-RBD (**A**) and MR17-RBD (**B**) were aligned to the closed conformation (PDB ID 6VXX)[2] of SARS-CoV-2 S protein. No significant clashes were observed for both sybodies. The three chains of S are colored yellow, white, and pale blue. Sybodies are colored blue.

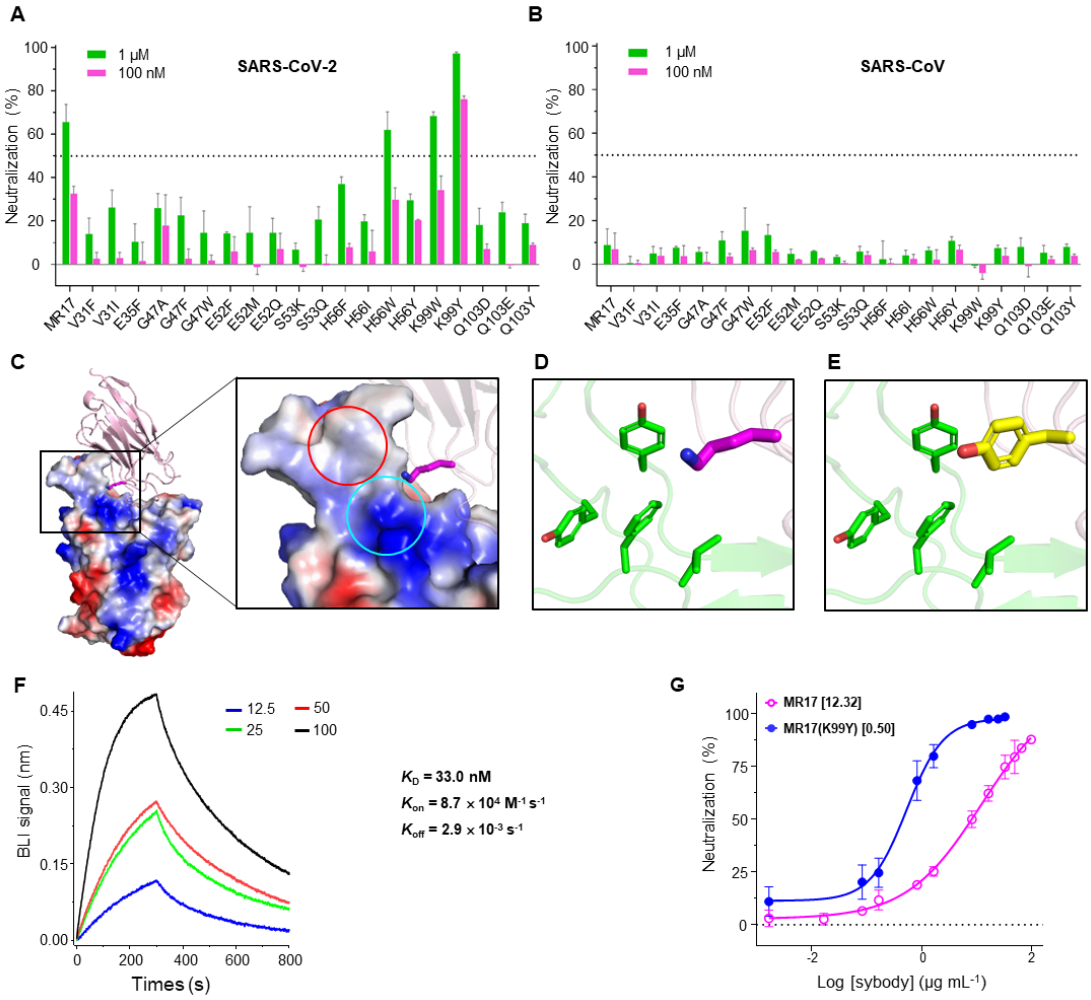

Extended Data Fig. 7. Structure-based design of a MR17 mutant (MR17m) with improved affinity and potency. (**A,B**) Neutralization assay for SARS-CoV-2 (**A**) or SARS-CoV (**B**) pseudotypes by the wild-type MR17 sybody and the 20 rationally designed single-mutants (See **Methods**). Sybody concentrations were used at 1 μM (green) and 100 nM (magenta) concentrations. Data are from three independent experiments. (**C,D**) Rational for the design of K99Y. The positively charged Lys99 pokes to an area (boxed) that contains a hydrophobic patch (red cycle) and a positively-charged surface (cyan cycle). Electrostatic repel and hydrophobic mismatch would make Lys99 unfavorable at this position. According to the original library design, Lys99 was unvaried[26], meaning that Lys99 was not *selected* and hence opportunities for optimization. (**E**) The K99Y mutation fits the hydrophobic microenvironment well, as revealed by the crystal structure of MR17m (**Extended Data Table 2**). (**F**) Binding kinetics of MR17m binding to RBD. BLI signals were recorded under indicated MR17m concentrations (nM). (**G**) Comparison of neutralization activity of MR17 and MR17m. IC_{50} values (μg mL^{-1}) for SARS-Cov-2 are indicated in brackets. Data for MR17 are from **Fig. 1B**. Data are from three independent experiments.

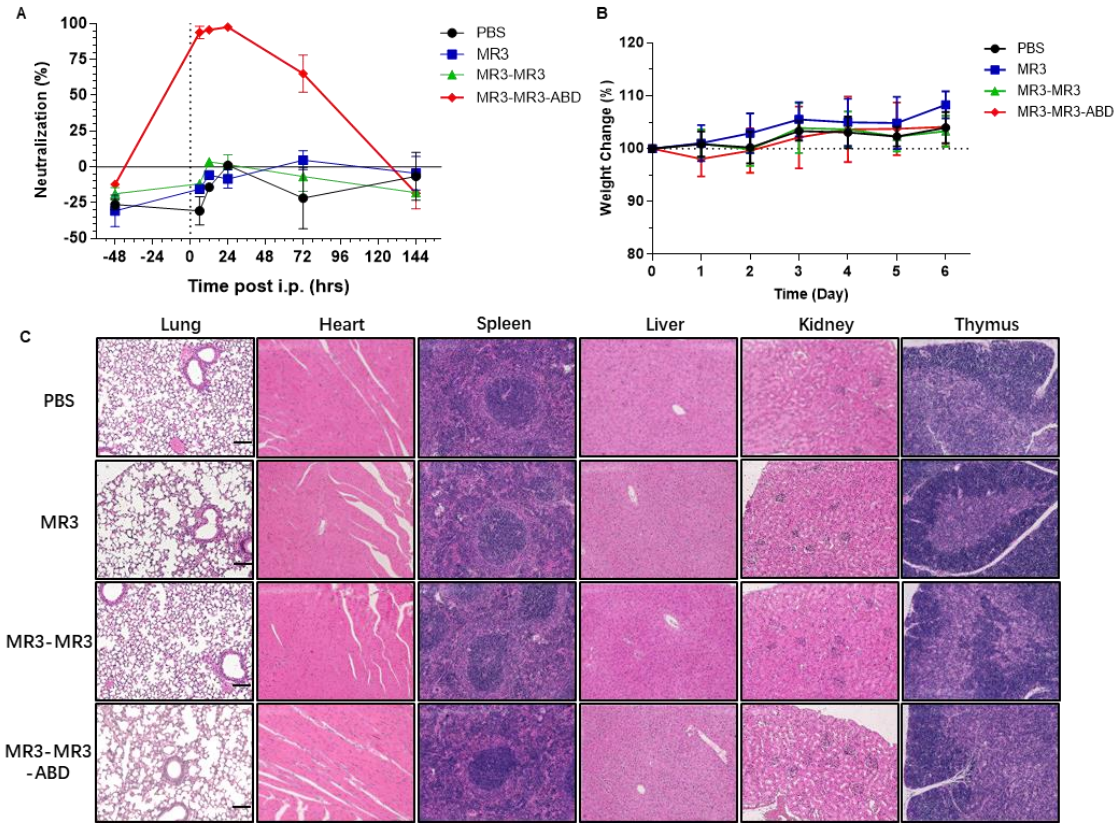

Extended Data Fig. 8. Evaluation of *in vivo* stability and toxicity of nanobodies. (**A**). Neutralization activity of sera from mice injected with sybodies. Sera were collected from mice injected with sybodies MR3, MR3-MR3, MR3-MR3-ABD, or PBS at the indicated time points. For neutralization assay, sera were preincubated with SARS-CoV-2 pseudovirus for 1 h before infection at 1/200 dilution. The infection rates on VeroE6-hACE2 were measure by FACS 3 days post infection. (**B**) Body weight changes. The body weight data are presented as means ± the SD of mice in each group (n= 4). No significant differences are observed. (**C**) Representative histopathology of the lungs, heart, liver, spleen, lungs, kidney, and thymus for the different sybodies injected. At day 3, the organ were collected, fixed, sliced and stain with hematoxylin and eosin. The images and areas of interest are magnified 100 ×. Bars indicate 100 μm.

771 **REFERENCES**

772

773 1 Wang, C., Horby, P. W., Hayden, F. G. & Gao, G. F. A novel coronavirus outbreak of global health
774 concern. *Lancet* **395**, 470-473, doi:10.1016/S0140-6736(20)30185-9 (2020).
775 2 Walls, A. C. *et al.* Structure, Function, and Antigenicity of the SARS-CoV-2 Spike Glycoprotein.
776 *Cell* **181**, 281-292.e286, doi:https://doi.org/10.1016/j.cell.2020.02.058 (2020).
777 3 Wrapp, D. *et al.* Cryo-EM structure of the 2019-nCoV spike in the prefusion conformation.
778 *Science* **367**, 1260-1263, doi:10.1126/science.abb2507 (2020).
779 4 Lan, J. *et al.* Structure of the SARS-CoV-2 spike receptor-binding domain bound to the ACE2
780 receptor. *Nature* **581**, 215-220, doi:10.1038/s41586-020-2180-5 (2020).
781 5 Shang, J. *et al.* Structural basis of receptor recognition by SARS-CoV-2. *Nature* **581**, 221-224,
782 doi:10.1038/s41586-020-2179-y (2020).
783 6 Wang, Q. *et al.* Structural and Functional Basis of SARS-CoV-2 Entry by Using Human ACE2. *Cell*
784 **181**, 894-904.e899, doi:https://doi.org/10.1016/j.cell.2020.03.045 (2020).
785 7 Yan, R. *et al.* Structural basis for the recognition of SARS-CoV-2 by full-length human ACE2.
786 *Science* **367**, 1444-1448, doi:10.1126/science.abb2762 (2020).
787 8 Wu, Y. *et al.* A noncompeting pair of human neutralizing antibodies block COVID-19 virus
788 binding to its receptor ACE2. *Science*, eabc2241, doi:10.1126/science.abc2241 (2020).
789 9 Cao, Y. *et al.* Potent neutralizing antibodies against SARS-CoV-2 identified by high-throughput
790 single-cell sequencing of convalescent patients' B cells. *Cell*,
791 doi:https://doi.org/10.1016/j.cell.2020.05.025 (2020).
792 10 Ju, B. *et al.* Human neutralizing antibodies elicited by SARS-CoV-2 infection. *Nature*,
793 doi:10.1038/s41586-020-2380-z (2020).
794 11 Vincke, C. *et al.* General strategy to humanize a camelid single-domain antibody and
795 identification of a universal humanized nanobody scaffold. *The Journal of biological chemistry*
796 **284**, 3273-3284, doi:10.1074/jbc.M806889200 (2009).
797 12 Rogers, T. F. *et al.* Isolation of potent SARS-CoV-2 neutralizing antibodies and protection from
798 disease in a small animal model. *Science*, eabc7520, doi:10.1126/science.abc7520 (2020).
799 13 Hansen, J. *et al.* Studies in humanized mice and convalescent humans yield a SARS-CoV-2
800 antibody cocktail. *Science*, eabd0827, doi:10.1126/science.abd0827 (2020).
801 14 Hanke, L. *et al.* An alpaca nanobody neutralizes SARS-CoV-2 by blocking receptor interaction.
802 *bioRxiv*, 2020.2006.2002.130161, doi:10.1101/2020.06.02.130161 (2020).
803 15 Huo, J. *et al.* Neutralizing nanobodies bind SARS-CoV-2 spike RBD and block interaction with
804 ACE2. *Nature Structural & Molecular Biology*, doi:10.1038/s41594-020-0469-6 (2020).
805 16 Custodio, T. *et al. Selection, biophysical and structural analysis of synthetic nanobodies that*
806 *effectively neutralize SARS-CoV-2*. (2020).
807 17 Walter, J. D. *et al.* Synthetic nanobodies targeting the SARS-CoV-2 receptor-binding domain.
808 *bioRxiv*, 2020.2004.2016.045419, doi:10.1101/2020.04.16.045419 (2020).
809 18 Schoof, M. *et al.* An ultra-high affinity synthetic nanobody blocks SARS-CoV-2 infection by
810 locking Spike into an inactive conformation. *bioRxiv*, 2020.2008.2008.238469,
811 doi:10.1101/2020.08.08.238469 (2020).
812 19 Van Heeke, G. *et al.* Nanobodies® as inhaled biotherapeutics for lung diseases. *Pharmacology*
813 *& therapeutics* **169**, 47-56, doi:10.1016/j.pharmthera.2016.06.012 (2017).
814 20 Nicola, M. *et al.* The socio-economic implications of the coronavirus pandemic (COVID-19): A

815 review. *Int J Surg* **78**, 185-193, doi:https://doi.org/10.1016/j.ijsu.2020.04.018 (2020).
816 21 Shang, J. *et al.* Cell entry mechanisms of SARS-CoV-2. *Proc Natl Acad Sci USA* **117**, 11727-11734,
817 doi:10.1073/pnas.2003138117 (2020).
818 22 Hoffmann, M. *et al.* SARS-CoV-2 Cell Entry Depends on ACE2 and TMPRSS2 and Is Blocked by a
819 Clinically Proven Protease Inhibitor. *Cell* **181**, 271-280.e278,
820 doi:https://doi.org/10.1016/j.cell.2020.02.052 (2020).
821 23 Robbiani, D. F. *et al.* Convergent antibody responses to SARS-CoV-2 in convalescent individuals.
822 *Nature* **584**, 437-442, doi:10.1038/s41586-020-2456-9 (2020).
823 24 Muyldermans, S. Nanobodies: Natural Single-Domain Antibodies. *Annu Rev Biochem* **82**, 775-
824 797, doi:10.1146/annurev-biochem-063011-092449 (2013).
825 25 McMahon, C. *et al.* Yeast surface display platform for rapid discovery of conformationally
826 selective nanobodies. *Nat Struct Mol Biol* **25**, 289-296, doi:10.1038/s41594-018-0028-6 (2018).
827 26 Zimmermann, I. *et al.* Synthetic single domain antibodies for the conformational trapping of
828 membrane proteins. *eLife* **7**, e34317, doi:10.7554/eLife.34317 (2018).
829 27 Zimmermann, I. *et al.* Generation of synthetic nanobodies against delicate proteins. *Nat Protoc*
830 **15**, 1707-1741, doi:10.1038/s41596-020-0304-x (2020).
831 28 Moutel, S. *et al.* NaLi-H1: A universal synthetic library of humanized nanobodies providing
832 highly functional antibodies and intrabodies. *eLife* **5**, e16228, doi:10.7554/eLife.16228 (2016).
833 29 Uchański, T. *et al.* An improved yeast surface display platform for the screening of nanobody
834 immune libraries. *Scientific Reports* **9**, 382, doi:10.1038/s41598-018-37212-3 (2019).
835 30 Custódio, T. F. *et al.* Selection, biophysical and structural analysis of synthetic nanobodies that
836 effectively neutralize SARS-CoV-2. *bioRxiv*, 2020.2006.2023.165415,
837 doi:10.1101/2020.06.23.165415 (2020).
838 31 Jovčevska, I. & Muyldermans, S. The Therapeutic Potential of Nanobodies. *BioDrugs : clinical*
839 *immunotherapeutics, biopharmaceuticals and gene therapy* **34**, 11-26, doi:10.1007/s40259-
840 019-00392-z (2020).
841 32 Krissinel, E. & Henrick, K. Inference of Macromolecular Assemblies from Crystalline State. *J Mol*
842 *Biol* **372**, 774-797, doi:https://doi.org/10.1016/j.jmb.2007.05.022 (2007).
843 33 Korber, B. *et al.* Tracking Changes in SARS-CoV-2 Spike: Evidence that D614G Increases
844 Infectivity of the COVID-19 Virus. *Cell* **182**, 812-827.e819,
845 doi:https://doi.org/10.1016/j.cell.2020.06.043 (2020).
846 34 Doud, M. B., Hensley, S. E. & Bloom, J. D. Complete mapping of viral escape from neutralizing
847 antibodies. *PLoS Pathog* **13**, e1006271-e1006271, doi:10.1371/journal.ppat.1006271 (2017).
848 35 Doud, M. B., Lee, J. M. & Bloom, J. D. How single mutations affect viral escape from broad and
849 narrow antibodies to H1 influenza hemagglutinin. *Nat Commun* **9**, 1386-1386,
850 doi:10.1038/s41467-018-03665-3 (2018).
851 36 Rockx, B. *et al.* Structural basis for potent cross-neutralizing human monoclonal antibody
852 protection against lethal human and zoonotic severe acute respiratory syndrome coronavirus
853 challenge. *J Virol* **82**, 3220-3235, doi:10.1128/JVI.02377-07 (2008).
854 37 ter Meulen, J. *et al.* Human Monoclonal Antibody Combination against SARS Coronavirus:
855 Synergy and Coverage of Escape Mutants. *PLOS Medicine* **3**, e237,
856 doi:10.1371/journal.pmed.0030237 (2006).
857 38 Tijink, B. M. *et al.* Improved tumor targeting of anti-epidermal growth factor receptor
858 Nanobodies through albumin binding: taking advantage of modular Nanobody technology.

Molecular cancer therapeutics **7**, 2288-2297, doi:10.1158/1535-7163.Mct-07-2384 (2008).

39 Jacobs, S. *et al.* Fusion to a highly stable consensus albumin binding domain allows for tunable pharmacokinetics. *Protein engineering, design & selection : PEDS* **28**, doi:10.1093/protein/gzv040 (2015).

40 Sun, J. *et al.* Generation of a Broadly Useful Model for COVID-19 Pathogenesis, Vaccination, and Treatment. *Cell* **182**, 734-743.e735, doi:https://doi.org/10.1016/j.cell.2020.06.010 (2020).

41 Shi, R. *et al.* A human neutralizing antibody targets the receptor-binding site of SARS-CoV-2. *Nature* **584**, 120-124, doi:10.1038/s41586-020-2381-y (2020).

42 Hassan, A. O. *et al.* A SARS-CoV-2 Infection Model in Mice Demonstrates Protection by Neutralizing Antibodies. *Cell* **182**, 744-753.e744, doi:https://doi.org/10.1016/j.cell.2020.06.011 (2020).

43 Gibson, D. G. *et al.* Enzymatic assembly of DNA molecules up to several hundred kilobases. *Nat Methods* **6**, 343-345, doi:10.1038/nmeth.1318 (2009).

44 Hattori, M., Hibbs, R. E. & Gouaux, E. A fluorescence-detection size-exclusion chromatography-based thermostability assay for membrane protein precrystallization screening. *Structure* **20**, 1293-1299, doi:10.1016/j.str.2012.06.009 (2012).

45 Zhang, W.-Z. *et al.* The protein complex crystallography beamline (BL19U1) at the Shanghai Synchrotron Radiation Facility. *Nucl Sci Tech* **30**, 170, doi:10.1007/s41365-019-0683-2 (2019).

46 Kabsch, W. XDS. *Acta Crystallogr D Biol Crystallogr* **66**, 125-132, doi:10.1107/S0907444909047337 (2010).

47 Evans, P. R. & Murshudov, G. N. How good are my data and what is the resolution? *Acta Crystallgr D* **69**, 1204-1214, doi:10.1107/S0907444913000061 (2013).

48 McCoy, A. J. *et al.* Phaser crystallographic software. *J Appl Crystallogr* **40**, 658-674, doi:doi:10.1107/S0021889807021206 (2007).

49 Emsley, P., Lohkamp, B., Scott, W. G. & Cowtan, K. Features and development of Coot. *Acta Crystallogr D* **66**, 486-501, doi:10.1107/s0907444910007493 (2010).

50 Adams, P. D. *et al.* PHENIX: a comprehensive Python-based system for macromolecular structure solution. *Acta Crystallogr D* **66**, 213-221, doi:doi:10.1107/S0907444909052925 (2010).

51 The PyMOL Molecular Graphics System, Version 2.0 Schrödinger, LLC. (Schrödinger, 2015).

52 Baker, N. A., Sept, D., Joseph, S., Holst, M. J. & McCammon, J. A. Electrostatics of nanosystems: Application to microtubules and the ribosome. *Proc Natl Acad Sci USA* **98**, 10037-10041, doi:10.1073/pnas.181342398 (2001).